Revealing the Effects of Nitrogen and non-radiative Auger Recombination Processes in $GaN_xAs_yP_{1-x-y}$/GaP type I QW by Hydrostatic Pressure

M.Sc.

in

Physics Engineering

University of Gaziantep

Supervisor

Prof. Dr. Beşire GÖNÜL

by

Shaza Ali YOUSF

August 2012

©2012 [Shaza A. YOUSF].

REPUBLIC OF TURKEY
UNIVERSITY OF GAZİANTEP
GRADUATE SCHOOL OF NATURAL & APPLIED SCIENCES
ENGINEERING PHYSICS

Name of the thesis: Revealing the Effects of Nitrogen and non-radiative Auger Recombination Processes in $GaN_xAs_yP_{1-x-y}/GaP$ type I QW by Hydrostatic Pressure

Name of the student: Shaza Ali YOUSF

Exam date: 29/ 08/ 2012

Approval of the Graduate School of Natural and Applied Sciences

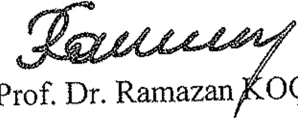

Prof. Dr. Ramazan KOÇ

Director

I certify that this thesis satisfies all the requirements as a thesis for the degree of Master of Science.

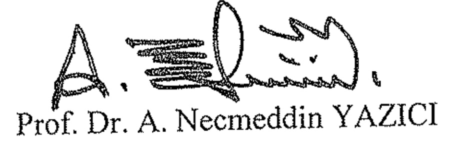

Prof. Dr. A. Necmeddin YAZICI

Head of Department

This is to certify that we have read this thesis and that in our consensus/majority opinion it is fully adequate, in scope and quality, as a thesis for the degree of Master of Science.

Prof. Dr. Beşire GÖNÜL

Supervisor

Examining Committee Members	Signature
Prof. Dr. Beşire GÖNÜL	…………
Assoc. Prof. Dr. Hüseyin TOKTAMIŞ	…………
Assoc. Prof. Dr. Koray KÖKSAL	…………

I hereby declare that all information in this document has been obtained and presented in accordance with academic rules and ethical conduct. I also declare that, as required by these rules and conduct, I have fully cited and referenced all material and results that are not original to this work.

Shaza YOUSF

ABSTRACT

Revealing the Effects of Nitrogen and non-radiative Auger Recombination Processes in $GaN_xAs_yP_{1-x-y}/GaP$ type I QW by Hydrostatic Pressure

YOUSF, Shaza

M.Sc. in Physics Engineering

Supervisor: Prof. Dr. Beşire GÖNÜL

August 2012, 65 pages

This thesis study investigates the important loss mechanisms in a newly proposed $GaN_xAs_{0.8}P_{0.2-x}/GaP$ type I QW laser system on a silicon substrate. Our calculations indicate that direct CHSH Auger loss mechanism is the most important loss mechanism in the QW laser system under investigation.

Key words: N concentration, hydrostatic pressure, effective mass, non-radiative Auger recombination.

ÖZET

$GaN_xAs_yP_{1-x-y}/GaP$ Tip I Kuvantum Kuyularında Nitrojen ve Işımasız Auger Etkisinin Hidrostatik Basınç ile Açığa Çıkarılması

YOUSF, Shaza

Yüksek Lisans Tezi, Fizik Müh. Bölümü

Tez Yöneticisi: Prof. Dr. Beşire GÖNÜL

Ağustos 2012, 65 sayfa

Bu tez çalışması yeni önerilen $GaN_xAs_{0.8}P_{0.2-x}/GaP$ kuvantum kuyu lazer sistemlerindeki önemli kayıp mekanizmalarını araştırmıştır. Hesaplamalarımız, araştırılan kuvantum kuyu lazer sistemlerinde en önemli kayıp mekanizmasının direk CHSH Auger kayıp mekanizması olduğunu göstermiştir.

Anahtar kelimeler: N konsantrasyonu, hidrostatik basınç, etkin kütle, ışımasız Auger rekombinasyon

I dedicate this thesis to my dear Mom and Dad

ACKNOWLEDGEMENTS

I would like to profoundly thank my adviser, Professor Beşire GÖNÜL, for being an amazing mentor and allowing me to follow my research passions. Her vast knowledge in such a large number of areas never fails to impress, and her easy-going nature always makes working with her enjoyable. I think that her advising style has been very positive for my growth as a researcher, and has given me a great deal of independence and confidence. I have truly enjoyed my time in this work with my supervisor, and I am very grateful to her for supporting my interests and my work. I would also like to thank the members of my reading committee, Asst. Prof. Dr. Hüseyin TOKTAMIŞ and Asst. Prof. Dr. Koray KÖKSAL. I would like to thank my colleague Ömer L. ÜNSAL I am particularly grateful to him, benefiting from his knowledge and our discussions about theoretical and computer subjects for all of his advice and efforts.

My special thanks to my Mom and Dad are the best parents I could ever hope for, and their prayer, love, guidance and support have been my best inspiration. I can't thank them enough for everything that they have done. I thank my dear husband Abdullah for his supports and efforts; he deserves enormous amounts of my warmest appreciation. He has been so wonderful over the past two years that there are no words to describe how. And finally to all of my family members, they deserve a lot of thanks their helping me get to this point. I thank them all so much.

TABLE OF CONTENTS

Page

ABSTRACT .... **iii**

ÖZET .... **iv**

ACKNOWLEDGEMENTS .... **vi**

TABLE OF CONTENTS .... **vii**

LIST OF TABLES .... **x**

LIST OF FIGURES .... **xi**

LIST OF SYMBOLS .... **xiv**

1. INTRODUCTION **1**

1.1 Thesis Outline **7**

2. LITERATURE SURVEY **8**

2.1 Dilute Nitride Alloys **8**

2.2 Hydrostatic Pressure **9**

2.3 Effective Mass **10**

2.4 Auger Recombination **11**

3. THEORETICAL MODELS OF BAND STRUCTURE **12**

3.1 Theoretical Models **12**

3.1.1 Material parameters 12

3.1.2 Interpolation method (Vegard’s Law) 13

3.1.3 Temperature impacts 18

3.1.4 Strain impacts 18

3.1.5 Model solid theory 22

3.1.6 The band anti-crossing model (BAC) 26
3.1.7 Electron effective mass 27

4. STRUCTURAL AND ELECTRONIC PROPERTIES of GaNAsP/GaP QW 29

4.1. Binary Compounds GaAs and GaP 29

4.2 Ternary Compounds $GaAs_{1-y}P_y$ 31

4.3 Quaternary Compound GaNAsP 32

4.4 Model Calculations of GaNAsP/GaP 34
4.4.1 Material parameters of GaNAsP QW 34
4.4.2 Parameters within BAC model for GaNAsP QW 35
4.4.3 Conduction band electron effective mass and N content 39

5. INVESTIGATION OF THE NITROGEN DEPENDENCE OF THE NON-RADIATIVE LOSS MECHANISMS IN $GaN_xAs_yP_{1-x-y}$/GaP 41

5.1 Introduction 41

5.2 Types of non-radiative Auger recombination process 41
5.2.1 Direct Auger process 42
5.2.2 Phonon-assisted Auger processes 45

5.3 Results and Conclusions 47

6. ANALYSIS OF THE PRESSURE DEPENDENCE OF BAND STRUCTURE AND AUGER LOSSES IN $GaN_xAs_{0.8}P_{0.2-x}$/GaP QW 48

6.1 Introduction 48

6.2 Pressure Dependence of Parameters 49

6.3 Results and Conclusions 49
6.3.1 Analysis of BAC model with pressure in $GaN_xAs_{0.8}P_{0.2-x}$/GaP 49
6.3.2 Hydrostatic pressure dependence of strained band gap 52
6.3.3 Investigation of the pressure dependence of electron effective mass 53
6.3.4 The analysis of the pressure dependence of non-radiative Auger recombination 55
6.3.4.1 Direct Auger processes (CHCC and CHSH) 56
6.3.4.2 Phonon-assisted Auger processes (CHCC and CHSH) 57

7. CONCLUSIONS 60

LIST OF REFRENCES 61

LIST OF TABLES

Page

Table 3.1: Binary alloy parameters for band structure calculations........................... 13
Table 3.2: Properties of elements of interest from groups V, including electronic structure, atomic mass, covalent radius and Pauling's electronegativity......... 15
Table 6.1: Linear and non-linear pressure coefficients.. 50

LIST OF FIGURES

Page

Figure 1.1: Band gap energy as a function of lattice constant. The grey boxes indicate nitrogen-containing alloys that have been grown lattice matched to Ge.. 4

Figure 1.2: Schematic representation of type-I and II band alignments. The black arrows show the band gaps and band of offsets. (a) Type I, (b) Type-II. 5

Figure 3.1: Electronegativity of the elements as a function of atomic number.. 16

Figure 3.2: Elastically growth (a) tensile-strained and (b) compressively-strained... 19

layers grown on thick substrates.. 19

Figure 3.3: Schematic diagram showing the bulk band structure of three $In_{1-x}Ga_xAs$ ternary strained layers grown on InP substrate.. 21

Figure 3.4: Diagram of the locations of confined states in strained and unstrained Quantum Well structures. In the right and left figures, only the well material is supposed to be strained. $E^{w}_{\Gamma,hh}$ is the bulk band edge of the well material. 21

Figure 3.5 Schematic energy band line-up of quantum well structure. 23

Figure 3.6: Band line-up of strained semiconductor (a) compressively strained, (b) lattice matched, and (c) tensiley strained layer. 25

Figure 3.7: A schematic diagram of a $GaAs_{0.58}P_{0.4}N_{0.02}$ HMA illustrating the splitting of the original conduction band E_M into E_+ and E_- due to the interaction of the N level E_N with E_M 28

Figure 4.1 3D crystal structure of zinc blende a) Gallium Arsenide, GaAs, and b) Gallium Phosphide, GaP. 30

Figure 4.2: Band structure of a) GaAs and b) GaP , respectively.. 30

Figure 4.3: Schematic band structure of GaAs, $GaAs_{1-y}P_y$ and GaP, respectively.. .. 31

Figure 4.4: Calculated energy positions of the Γ (solid line) and X (dashed line) conduction bands of the $GaAs_{1-y}P_y$ alloy system, direct-indirect crossover occurs at 0.5% P composition. 32

Figure 4.5: Energy gap versus the lattice constant of the most common III–V semiconductors in comparison to Si.. 34
Figure 4.6: Calculated subband energies E_- and E_+ versus nitrogen concentration for $GaN_xAs_yP_{1-x-y}$ on GaP substrate, according to BAC model. The difference between E_- and E_+ energies strongly depends on the N composition, the splitting up increases approximately linearly with x in the calculated concentration range 37
Figure 4.7: The calculated strain in well with respect to the nitrogen concentration in GaNAsP/GaP QW. 37
Figure 4.8: The strain in well as a function of As in $GaN_xAs_yP_{1-x-y}$/GaP QW 38
Figure 4.9: Band gap energy versus N concentration. E_{c-hh} is the strained energy and E_- is the lower subband according to band anti-crossing model. 39
Figure 4.10: Electron effective mass of conduction band as a function of nitrogen concentration. 40
Figure 5.1: Schematic diagram of Auger recombination process. 42
Figure 5.2: CHCC, CHHS Auger process in a quantum well.. 43
Figure 5.3: The normalized Auger rate as a function of N concentration for four types of Auger recombination processes for $GaN_xAs_{0.8}P_{0.2-x}$. 47
Figure 6.1: Pressure dependence of the energy for $GaN_{0.04}As_{0.8}P_{0.2-x}$ QW lasers. The pressure dependence of the GaAsP conduction band (E_M) is also shown. 51
Figure 6.2: The calculated dispersion of the E_- and E_+ subbands at three different pressures.. 52
Figure 6.3: Strained band gap energy with pressure for different values of N concentration (x), $GaN_xAs_{0.8}P_{0.2-x}$/GaP QW. 53
Figure 6.4: Electron effective mass as a function of pressure for various N concentrations. 54
Figure 6.6: The calculated values of electron effective mass with increasing nitrogen and pressure for $GaN_xAs_{0.7}P_{0.3-x}$ QW on GaP substrate, according to BAC model 55
Figure 6.7: Direct Auger processes (CHCC) as a function of pressure for different values of N concentrations (x) in $GaN_xAs_{0.8}P_{0.2-x}$ on GaP substrate. 56
Figure 6.8: Direct Auger processes CHSH as a function of pressure with different N concentrations (x) $GaN_xAs_{0.8}P_{0.2-x}$ on a GaP substrate. 57

Figure 6.9: Phonon-assisted Auger processes CHCC as a function of pressure with different N concentrations (x). 58
Figure 6.10: Phonon-assisted Auger processes CHSH as a function of pressure with different N concentrations (x). 58
Figure 6.11: Auger processes (CHCC and CHSH) for both direct and phonon-assisted as a function of pressure with N concentrations (x=0.1). 59

LIST OF SYMBOLS

Abbreviations:

HMAs	**H**ighly **M**ismatched **A**lloys
MQWHs	**M**ulti **Q**uantum **W**ell **H**eterostructures
MOVPE	**M**etalorganic **V**apour **P**hase **E**pitaxy
QW	**Q**uantum **W**ell
DBR	Distributed **B**ragg **R**eflector
BZ	**B**rillouin **Z**one
AR	**A**uger **R**ecombination
BAC	**B**and **A**nticrossing Model
MOCVD	**M**etal **O**rganic **C**hemical **V**apour **D**eposition
MBE	**M**olecular **B**eam **E**pitaxy
CB	**C**onduction **B**and
VB	**V**alence **B**and
DFT	**D**ensity **F**unctional **T**heory
CS	**C**luster **S**tate
CBM	**C**onduction-**b**and **M**inimum
DOS	**D**ensity **o**f **S**tate
LED	**L**ight **E**mitting **D**iode
SC	**S**olar **C**ell
ZB	**Z**inc **B**lende

Latin Symbols:

E_g	Band gap
a_o	Lattice constant
a_e	Lattice constant of epitaxial layer
a_s	Lattice constant of substrate
T_o	Temperature
k_B	Boltzmann's constant
C	Auger Coefficient
Δ_o	Spin-orbit Splitting
a_c	Hydrostatic deformation potential for conduction band
a_v	Hydrostatic deformation potential for valence band
C_{11}	Elasti Stiffness Constant
C_{12}	Elasti Stiffness Constant
d	Deformation Potential
$E_{v,av}$	The average valence subband energy
$\Delta E_{c,v}$	The band discontinuities for conduction and valence band
E_c	Conduction band energy (eV)
E_v	Valence band energy (eV)
$Q_{c,v}$	The band offset ratio for conduction and valence band
$\delta E_c(x,y)$	The shifted conduction band energy
E_M	Conduction state of the matrix semiconductor
E_N	Localized nitrogen state energy
V_{MN}	The matrix element describing the coupling effect
C_{MN}	Coupling constant
$E_{\pm}$	Conduction band energy state
m_M	The matrix semiconductor effective mass

m_o	Free electron mass
m*	The electron effective mass due to the N incorporation
m_c	Electron effective mass for conduction band
m_{hh}	Valence band (heavy hole) effective mass
m_{lh}	Valence band (light hole) effective mass
m_s	Spin-split-off band
e	Electron charge
k	Wavevector
E_{c-hh}	The strained energy in the conduction band
E_a	Activation energy
$\|M_{ee}\|$	Electron-electron interaction matrix element
$f_{CH,SH}$	Oscillator strength
E_p	The equivalent energy of the momentum matrix element
M	The sum of the masses of the atoms
A	The area of the QW
v_s	The velocity of light

Greek Symbols:

β	Varshni parameters
$\varepsilon_{\|\|}$	strain
ε_{vol}	The hydrostatic constituent
ℏ	Plank's constant
γ_1, γ_2	Luttinger parameters
ω	Angular frequency of light
μ	Dipole moment along a given polarisation of light
Ω_o	The elementary cell of volume

CHAPTER 1

INTRODUCTION

Year middle of 1960s, the communications engineering realized that the existing copper wire infrastructure used to transfer voice and data would not have enough bandwidth for the impending increase in traffic. This requires an intensive international attempt to find a solution to overcome copper's limitations. The use of laser beam seemed very promising, especially for the large bandwidth that would be available.

Among the different solutions experimented, in 1966 a technique was proposed that used a continuous glass fiber as a guidance system to transmit light signals, optical fiber communication was born. But it was only with the beginning of "information technology". In the last two decades, that optical fiber communication has become firmly established in most countries of the world.

The structure of an optical communication channel is similar to other types of communication system: a transmitter, that contains an optical source and a means of modulating the output with the signal to be transmitted; a transmission medium in which the informations travels; a receiver, where the optical signal is changed first in an electrical waveform and then in a form suitable for use.

One of the main problems in an optical fibre communications technology is the reduction of the signal along the transfer. By developing ways to eliminate absorbing impurities from the fibre, it was possible to reach very low absorption in the infrared region of the electromagnetic spectrum, inside two windows centred at 1.3 and

1.55μm. For this reason, great interest had the development of long-wavelength semiconductor lasers working at these minima, such as III-N-V alloys.

Recently, the semiconductors can be developed with varying mole fraction of a few atomic layers at a time. Hence the number of achievable new electronic devices and materials is increasing much more. Semiconductor devices have been widely used in different range from microelectronics to optoelectronic devices and chemical sensors. The material types of semiconductor include elemental semiconductors (Si, Ge), compound (III–V) semiconductors (GaAs, GaP, InP, etc.…) [1]. A remarkable growth in the technology of dilute nitrides pronounced, leading to a great number of device concepts and scientific reports. Dilute nitrides contain (nitrogen anion-mixed III–V ternary and quaternary alloys) for example GaPN, GaAsN, or GaNAsP are derived from conventional III–V semiconductors such as GaAs, GaP, or InGaAs by the incorporation of nitrogen into the group V sublattice.

The beginning of the nitride semiconductor start of 1990s, stirred by the success in the fabrication of best III–V semiconductor alloys based on (Ga, Al, In) (P, As), as well as they penetrate in growth of wide-band-gap III-nitrides. The main stimulation by that time was to reduce the gap between the arsenide and the nitrides, this lead to produce light emitters covering the whole visible spectral range based on the direct band-gap materials [2].

Dilute nitrides in fact belonged to a novel class of highly mismatched semiconductor alloys (HMAs) with noticeably unusual physical properties. These properties were clearly dissimilar from conventional semiconductor alloys and were found attractive in optoelectronic semiconductor device applications [2]. Unlike III-V conventional alloy semiconductor, where the energy of the band-gap alloys can be practically approximated as a weighted linear average of the band gaps of their parental compounds, dilute nitrides show a huge bowing of the band-gap energy due to a strong mismatch in electronegativity and atomic size between nitrogen atom and the replaced anion atom.

The novel material system has many significant advantages for laser applications when compared to the most commonly used InGaAsP/InP systems:

a) The structures of laser established a good high temperature performance due to the larger conduction band offset. Thus it reduces the electron leak out at room temperature and above, this leads to improve electron confinement.
b) Nitrogen implantation increases the effective mass of electron in the conduction band; it provides a close match between the effective mass value for both of electrons and holes in the conduction and valence band, respectively. This type of system called novel material system.

Band gap (E_g) and lattice constant (a_o) are affected from nitrogen incorporation into the III-V alloy semiconductor. It causes a reduction in band gap and decreases the lattice constant, unlike the addition of Ga, In, P, As, Sb where a reduction (increase) in band gap energy is achieved by increasing (decreasing) the lattice constant.

Figure 1.1 shows the relationship between a_o and E_g for conventional III-V and novel III-N-V alloy semiconductors, such as $Al_xGa_{1-x}As$, $Ga_{1-x}In_xAs$, $Ga_{1-x}In_xP$, GaAsN etc. Nowadays, As-rich dilute nitride compressively strained (GaNAsP) multiquantum well heterostructures (MQWHs) were grown on GaP-substrates by metalorganic vapour phase epitaxy (MOVPE) without any misfit dislocation formation [3]. These heterostructures can be considered as novel material systems and they can be used as a suitable light emitters [4.]

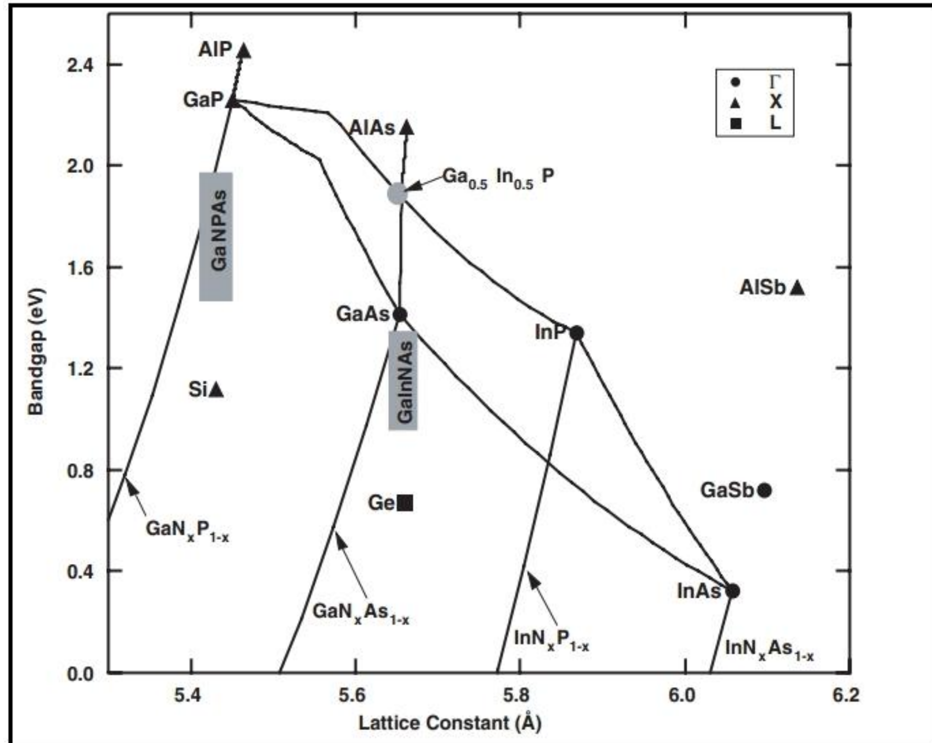

Figure 1.1: Band gap energy as a function of lattice constant. The grey boxes indicate nitrogen-containing alloys that have been grown lattice matched to Ge [5].

In type I quantum well (QW) band lineup, which is necessary for an efficient light emission, both electrons and holes are confined to the QW layer. Addition of N into InGaAs has allowed the growth of nitride semiconductor alloy having much longer emission wavelengths than that of GaAs. GaInNAs has enabled the development of lasers at the important fibre communication wavelength of 1.3 µm with some advantages of [6];

i. Conduction band well is deeper providing better confinement of electrons.
ii. Electron effective mass is larger resulting better match of the valance and conduction-band densities of states.
iii. GaInNAs/GaAs lasers have excellent high-temperature performance, higher T_o, higher efficiency and output power.
iv. The stability of the lasing wavelength is excellent despite the changes in temperature.
v. The operation speed is high.

vi. GaInNAs/GaAs lasers can be grown on a highly reflective GaAs/AlAs Distributed Bragg Reflector (DBR) mirror over a GaAs substrate in a single stage of epitaxial growth.

The value quantifying the alignment of the valence bands of two semiconductors is called the valence band offset. This is an important parameter characterizing a heterostructure. There are several types of band alignments; the two major ones are called type-I and type-II. Figure 1.2 shows these two types of band alignment for a superlattice made of two arbitrary semiconductor materials A and B of band gaps E_g^A and E_g^B, respectively. We are going to investigate the GaNAsP / GaP type I QW in this thesis.

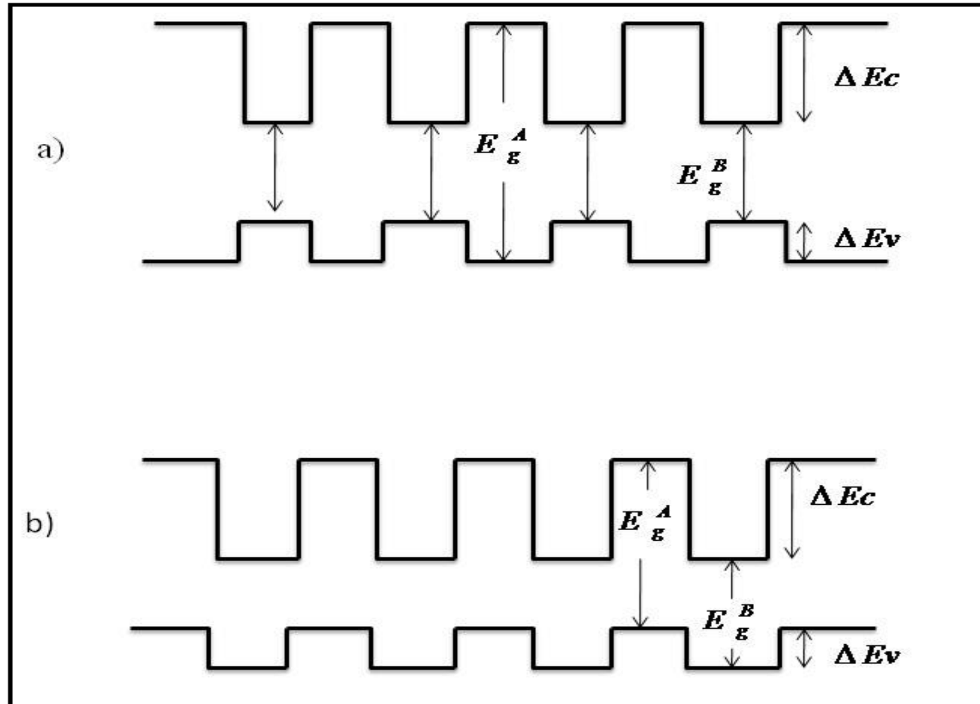

Figure 1.2: Schematic representation of type-I and II band alignments. The black arrows show the band gaps and band of offsets. (a) Type I, (b) Type-II.

Hydrostatic pressure is an important tool to investigate the loss mechanisms in semiconductor optoelectronic device such as Auger recombination processes. The direct band gap of the semiconductor is increasing at a rate of about 10meV/kbar, hence decreasing the emission wavelength of the lasers.

The loss mechanisms in semiconductor lasers are strongly wavelength dependent. In tetrahedral semiconductor i.e. groups (IV, III-V and II-VI) the effect of hydrostatic pressure decreases the crystal lattice constant and consequently increases band gap (E_g) throughout the Brillouin zone (BZ). Applied hydrostatic pressure changes the band structure qualitatively without changing the crystal symmetry [7].

Hydrostatic pressure provides a convenient method to vary continuously the band structure of semiconductor lasers [8]. In nitride semiconductor the same behaviour has happened with a hydrostatic pressure in band structure, it has an identical effect on the band gap, while the band gap goes down by increases N content in alloys. Effective mass increases also by nitrogen incorporation into the alloy. This thesis reveals the effects of nitrogen and hydrostatic pressure in $GaN_xAs_yP_{1-x-y}$/GaP type I QW, which impact on the strained band gap, electron effective mass m_e^* and non-radiative Auger recombination processes (AR).

Hydrostatic pressure can be used to continually fluctuate the emission energy of a laser enabling the study of band gap dependent processes. This is a reasonable alternative method to grow a group of device with altering material parameters which eliminates the effects that distinction in growth quality and compositions between the structures that may have an effect on device performance.

The band structure is another necessary factor in the analysis of important optoelectronic device properties. The band structure parameters are dependent on external influence such as, temperature and pressure.

In III-N-V semiconductor band structure calculation, several theoretical expressions and models have been used to describe these types of materials. There are Vegard's law (Interpolation method), band anticrossing (BAC), Pikus-Bir Hamiltonian for strained QW band structure, etc.

The objective of this thesis is to reveal the hydrostatic pressure impacts on the band structure of selected ($GaN_xAs_{0.8}P_{0.2-x}$/GaP) type I QW laser. The effect of pressure on strained band gap energy, electron effective mass m_e^* and Auger recombination processes will be examined in detail.

1.1 Thesis Outline

Chapter 1: Introduction

Chapter 2: Literature survey summarizes the nitride semiconductor properties according to the N incorporation and hydrostatic pressure of III-N-V alloy semiconductors.

Chapter 3: The theoretical models will be presented. The band structure and material parameters which are used throughout the thesis for III-V nitride QW laser systems will be provided.

Chapter 4: This chapter first illustrates the band structure and electronic properties of conventional alloy $GaAs_{1-y}P_y/GaP$ QW. Then we show the effects of N incorporation into the selected material system of $GaN_xAs_{0.8}P_{0.2-x}/GaP$ QW with the calculated models.

Chapter 5: It investigates the nitrogen dependence of the non-radiative loss mechanisms of Auger recombination in $GaN_xAs_{0.8}P_{0.2-x}/GaP$ QW. This property depends on the different values of nitrogen concentration of the band structure.

Chapter 6: This chapter deals with the influence of hydrostatic pressure in the band structure of $GaN_xAs_{0.8}P_{0.2-x}/GaP$ QW, especially with loss mechanism.

Chapter 7: Conclusion.

CHAPTER 2

LITERATURE SURVEY

2.1 Dilute Nitride Alloys

The first GaAsN alloy with an N concentration of 1.6% was grown by Weyers et al.(1992) by means of metalorganic chemical vapour deposition (MOCVD) at low pressure. The N source was derived by decomposing NH_3 in remote microwave plasma. They observed a strong band gap reduction of the alloys [9].

Kondow and co-workers (1994) revealed that the addition dilute amounts of N to GaAs (InGaAs) to form GaNAs (GaInNAs) dramatically reduced the band gap [10]. This allows the opportunity to get much longer wavelengths. It is expected that the InGaAsN material brings advantages over the InGaAsP, due to the more favourable band offsets and consequently better laser operation characteristics. This gives best result as to fabricate long wavelength material compared to InGaAsP, which was used to design for the 1.3 μm wavelength. The outcome contradicted the general trend of all previously studied III-V alloys that small lattice constant alloys have large band gaps. Kondow et al. suggested that InGaAsN could be grown lattice matched with GaAs substrates

Walukiewicz et al. (1999) investigated that the N implantation into the III-V semiconductor leads to dividing (splitting) the conduction band of the host alloy into two subbands. The splitting can be described in terms of an anticrossing interaction between a narrow band of localized nitrogen states and the extensive conduction-band states of the alloys matrix. They proved that the modification of the conduction-

band structure strongly affects the optical and electrical properties of the III-N-V semiconductor [11].

Bi et al. (1996) grew GaAsN with N composition of 14.8% on GaP by MBE under low growth temperature. This is the highest N composition obtained till now [12].

Toivonen et al. (2000) reported their growth of GaAsN alloys with a N composition of 5.6% by MOCVD [13].

2.2 Hydrostatic Pressure

Perlin et al. (1992) showed the theoretical and experimental studies of the essential electronic properties of III-V nitride. In this study they grew single crystals of nitrides used for the resolution of optical and structural properties, it's grown by an equilibrium high-pressure technique [14].

Shan et al. (1999) suggested a"band anticrossing" (BAC) model for describing dilute nitride alloys. BAC takes into account the nitrogen states leads to strong interaction between a narrow resonant band and the conduction band. It explained well the fundamental band gap change under hydrostatic pressure. The significant and convenient advantage of the BAC model is that it provides uncomplicated analytic expressions for the conduction band (CB) splitting [15]. This allows to simply calculating, the transition energies between electronic states in Quantum wells or the gain in laser structures, the oscillator strength of the optical transitions in bulk material, etc.

In the study of Christensen et al. (2003) they focused on the various defect levels under hydrostatic pressure, and they explained the distinction of defect formation energies with applied pressure [16].

Gorczyca et al. (2005) examined the electronic structures of $GaAs_{1-x}N_x$ semiconductor within the density functional theory (DFT). They also examined the impacts of applying external pressure and of changing the concentration, x. The

incorporation of nitrogen modified the X and L in the Brillouin zone near the host conduction bands. Their interaction with the lowest conduction a band induces a prominent non-parabolicity for this band and affects profoundly the value of the electron effective mass [17].

Wu et al. (2001) experimentally explained the dispersion relationship. Their results were dependent on nitrogen, they observe a huge increase in the effective mass of electron [18].

Gönül et al. (2004) compared the effects of applied pressure upon the threshold carrier and current density for three typical competing laser devices (InGaAsP–InP, AlGaInAs–InP and InGaAsN–GaAs) emitting in the approximately of 1.3 μm. The difference of pressure dependence of laser parameters indicates that N- and Al-based laser systems are better than the P-based laser system. They also showed that an Al- and N-based laser system was a perfect option for high-speed applications and low threshold, respectively [19].

Klar et al. (2007) explained and found that under applied hydrostatic pressure, the conduction band edge is shifted to upper energies at a rapid rate, so the localized state of N near band gap, which is called also cluster state (high nitrogen localized cluster state) reemerge into the gap. This reflects the low pressure coefficient of the cluster state, due to their weak hybridization with the perturbed host states [20].

Chamings et al. (2008) found that the band anticrossing model could better illustrate the band gap of GaNAsP/GaP as a function of pressure. In addition, they found that carrier leakage acting a great role in GaNAsP lasers. They studied their experiments under different values of temperatures [21].

2.3 Effective Mass

Skierbiszewski et al (1999) proved experimentally that by taking into account the conduction band's strong non-parabolicity, the effective mass in GaAsN/GaAs

quantum wells increases from $0.095m_o$ to $0.115m_o$ for a nitrogen content varying from 1% to 3% [22].

Hung et al. (2002) explained the large enhancement of the effective mass due to the N incorporation. They recognized that this is mainly due to the nitrogen caused adjustment on the electronic states near the edge of the conduction band [23].

2.4 Auger Recombination

Jin et al. (2003) noticed an abnormal increase of the non-radiative Auger recombination current with rising pressure in GaInNAs, which is different to those in 1.3μm InP-based AlGaInAs andInGaAsP devices, where the Auger current reduce with pressure. This is due to a huge increase in the threshold carrier density with rising pressure in GaInNAs [24].

Massé et al. showed that the band gap dependence of the internal losses plays an important role in the band gap dependence of the radiative current. Temperature dependence calculations show that at room temperature, the radiative current accounts for 20% of the total threshold current. This allows them to determine the pressure dependence of the non-radiative Auger recombination current, and hence to experimentally get the difference of the Auger coefficient C with band gap [25].

CHAPTER 3

THEORETICAL MODELS OF BAND STRUCTURE

3.1 Theoretical Models

A theoretical model is a hypothesis planned to describe the whole circumstances or performance, with the idea that it would eventually be able to expect that performance. The aim of this chapter is to illustrate and express several of these models, which are related to the band structure properties and material parameters of the QW laser system.

3.1.1 Material parameters

Material parameters have an important function in theoretical model's calculations. The lattice constant, effective masses, elastic stiffness constants and strain-related parameters of the conventional ternary and quaternary are calculated by linear interpolation method [26]. The constant values of the related binary alloys are tabulated in table 3.1.

Band structure material parameters are the most important commonly measured and calculated ones and they include [26]:

I. Direct and indirect energy gap.
II. Crystal-field splitting for nitrides
III. Spin-orbit splitting.
IV. Luttinger parameters and split-off hole mass.

V. Electron effective mass.

VI. Conduction and valence band deformation potentials that account for strain effects.

VII. Band offsets on an absolute scale which allows the band alignments between any combinations of materials to be determined.

Table 3.1: Binary alloy parameters for band structure calculations [6, 27, 28].

Material	**GaAs**	**GaN**	**GaP**	**InAs**	**InP**	**InN**	**AlAs**
Lattice Constant $a_o(\dot{A})$	5.6533	4.5	5.4505	6.0584	5.8697	4.98	5.661
Energy gap E_g(eV)	1.424	3.299	2.76	0.417	1.4236	0.78	3.099
Spin-orbit Splitting Δ_o (eV)	0.34	0.017	0.08	0.39	0.108	0.005	0.28
Hydrostatic deformation potential for CB a_c (eV)	-7.17	-6.71	-8.2	-5.08	-6.0	-2.65	-5.64
Hydrostatic deformation potential for VB a_v (eV)	-1.16	-0.69	-1.7	-1.0	-0.6	-0.7	-2.47
Elasti Stiffness Constant C_{11} (GPa)	1221.0	293.0	1405	832.9	1011.0	187.0	1250.0
Elasti Stiffness Constant C_{12} (GPa)	566.0	159.0	620.3	452.6	561.0	125.0	534.0
Deformation Potential b (eV)	-2.0	-2.0	-1.6	-1.8	-2.0	-1.2	-2.3
$E_{v,av}$	-6.92	0.0	-7.40	-6.67	-7.04	0.0	-7.49

3.1.2 Interpolation method (Vegard's Law)

The interpolation method which is called as the Vegard's law has been widely used in materials and mineralogy science since six decades. According to Vegard's law, unit cell parameters should vary linearly with concentration [29]. The law is suitable for ionic salts and compounds [30].

Optoelectronic devices base on binary material alloys. Because of the arbitrary distribution of elements of the similar group inside the alloy lattice, accurate measurements of material parameters are hardly probable.

The mainly important parameters of a semiconductor are the band gap and the lattice constant. To calculate the lattice constant of semiconductor alloys, the Vegard's law is usually employed [6].

The simplest mathematical expression of Vegard's law for a binary solid solution [29] (binary parameter A-B) is:

$$a=a_A^o(1-x)+a_B^o(x) \quad (3.1)$$

where $x=x_B$ is the component B concentration and a_A^o and a_B^o are the lattice constant parameters of pure components A and B, respectively.

The interpolation method used to determine material parameters for ternary, quaternary, quinary alloys as well. The ternary parameter (T) of the form $A_xB_{1-x}C$ is derived from binary parameters (B) by:

$$T_{ABC}(x)=xB_{AC}+(1-x)B_{BC} \quad (3.2)$$

Eqn.(3.2) can be written taking into account bowing as:

$$T_{ABC}(x)=xB_{AC}+(1-x)B_{BC}+Cx(1-x) \quad (3.3)$$

where C is called a "bowing'' or "non-liner'' parameter. For most III-V semiconductor alloy, band gap is usually smaller than the linear interpolation result and so C is positive. The energy band gap bowing in semiconductors has been associated to alloy disarray, with C values related to the electronegativity mismatch of the components [31].

Table 3.2 is a summary of the properties of Group V elements, including atomic mass, electronic structure, covalent radius, and Pauling's electronegativity.

Table 3.2: Properties of elements of interest from groups V, including electronic structure, atomic mass, covalent radius and Pauling's electronegativity [31].

Element	**Electronic structure**	**Atomic Mass**	**Covalent Radius (nm)**	**Electronegativity**
N	(He) $2s^2 2p^3$	14.007	0.07	3.04
P	(Ne) $3s^2 3p^3$	30.97	0.106	2.19
As	(Ar) $3d^{10} 4s^2 4p^3$	74.92	0.118	2.18
Ga	$4s\ ^2p^1$	69.723	0.126	1.81
In	$5s^2p^1$	114.818	0.144	1.78

The values of Ga and In are taken from Ref.[32,33].

Electronegativity of the elements is a significant property of which Pauling has been described in qualitative terms as "the power of an atom in a molecule to attract electrons to itself". [34]. Nitrogen has a large electronegativity according to the electronegativities of Ga, In, N, As, and P, they are 1.81, 1.78, 3.04, 2.18, and 2.19, respectively. The electronegativity values are plotted in Fig. 3.1 for most of the group II, III, VI, V and VI elements.

The large electronegativity of N leads to stronger electron localization around the N atom in III-N bonds compared to the column III atoms or even the As or Sb atoms in III-As or IlI-Sb bonds. Since these electronic states are localized in real space, they are spread out in momentum space and so flat energy-wave vector dispersion is assumed [6].

The location of the energy state is obtained from the nature and the strong point of the local potential known by the isovalent impurity. Hypothetical calculations obviously show that the energy levels of elements with high electronegativity are located at energies lesser than those of more-metallic impurities. Thus substitution of As with P give an energy level high in the conduction band of GaAs, whereas replacement of As with highly electronegative N produce located level close to the conduction-band minimum (CBM).

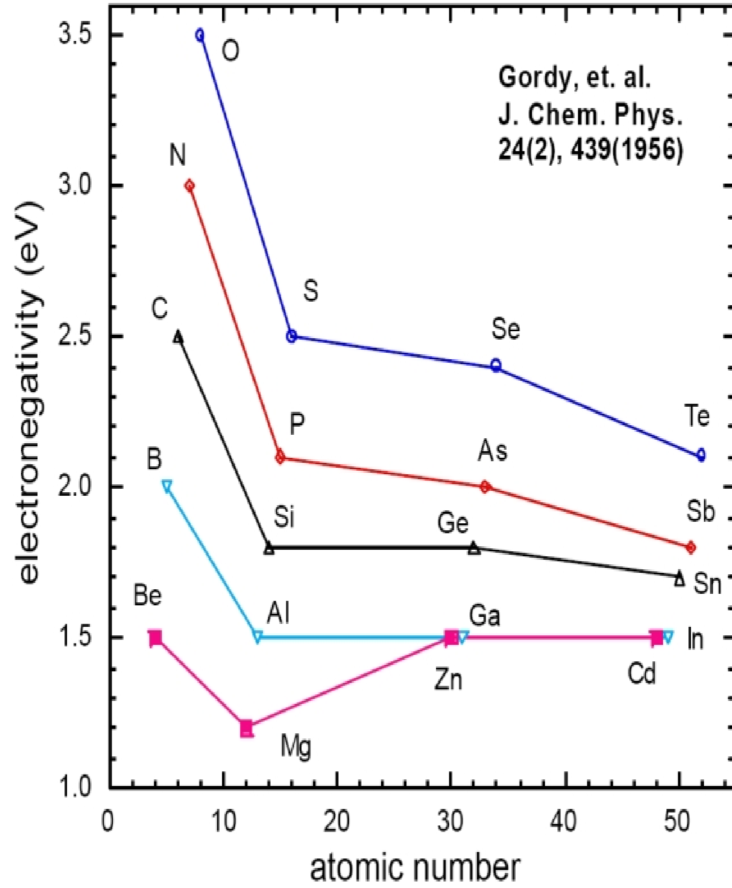

Figure 3.1: Electronegativity of the elements as a function of atomic number [6].

The quaternary material $A_{1-x}B_xC_yD_{1-y}$ is considered to be constructed of four binaries material: AC, AD, BC, and BD. If one uses a linear interpolation method, the quaternary parameter (Q) can be derived from the binary parameters by

$$Q(x,y)=(1-x)yB_{AC}+(1-x)(1-y)B_{AD}+xyB_{BC}+x(1-y)B_{BD} \tag{3.4}$$

If one of the four binary parameters is absent (e.g., B_{AD}), the quaternary parameter can be approximate from:

$$Q(x,y)=(1-x)B_{AC}+(x+y-1)B_{BC}+(1-y)B_{BD} \tag{3.5}$$

The quaternary material $A_{1-x}B_xC_yD_{1-y}$ is considered to be contained three binaries: AD, BD, and CD. The related linear interpolation can be written as:

$$Q(x,y)=xB_{AD}+yB_{BD}+(1\text{-}x\text{-}y)B_{CD} \tag{3.6}$$

If relationships for the ternary parameters (T's) are available, the quaternary parameter can be expressed either as($A_{1\text{-}x}B_xC_yD_{1\text{-}y}$) and ($A_x\ B_y\ C_{1-x-y}D$).

For $A1_{\text{-}x}B_xC_yD_{1\text{-}y}$ alloys:

$$Q(x,y)=\frac{x(1\text{-}x)[yT_{ABC}(x)+(1\text{-}y)T_{ABD}]+y(1\text{-}y)[xT_{ACD}(y)+(1\text{-}x)T_{BCD}]}{x(1\text{-}x)+y(1\text{-}y)} \tag{3.7}$$

while for ($A_x\ B_y\ C_{1-x-y}D$)

$$Q(x,y)=\frac{xyT_{ABD}(u)+y(1\text{-}x\text{-}y)T_{BCD}(v)+x(1\text{-}x\text{-}y)T_{ACD}(w)]}{xy+y(1\text{-}x\text{-}y)+x(1\text{-}x\text{-}y)} \tag{3.8}$$

with

$$u=\frac{1\text{-}x\text{-}y}{2},\qquad v=\frac{2\text{-}x\text{-}2y}{2},\qquad w=\frac{2\text{-}2x\text{-}y}{2}$$

For quinary alloys $D_{1\text{-}x}E_xF_y\ G_{1\text{-}y\text{-}z}H_z$, with a third column V element, the average can be find in terms of the nine ternary alloys (DEF, DEG, EFG, DFG, DFH, EFH, DGH, DEH and EG):

$$P_{DEFGH}=\frac{\sum c_{ijk}P_{ijk}}{\sum c_{ijk}} \tag{3.9}$$

where $c_{ijk} = xy(1 - x - y - z)$, are the fractional concentration mechanism for EFG. The ternary parameter P_{EFG} is calculated for the same F:G fraction as was present in the quinary.

3.1.3 Temperature impacts

Band gap energy strongly depends on the ambient temperature of the semiconductors. It tends to be decreased as the temperature is increased. This temperature-dependence involve in both direct and indirect band gaps. The origin of the temperature-dependent band gap is induced by thermal extension of the lattice and the changes in the electron-phonon interaction [6] Equation (3.10) which is called as Varshni formula, gives the temperature dependence of the band gap:

$$E_g(T)=E_g(0)-\frac{\alpha T^2}{T+\beta} \quad (3.10)$$

where $E_g(0)$ is the energy of band gap at T=0 K. α is in electron volts per Kelvin and β is directly associated to the Debye temperature of the substance (in Kelvin), they also called as Varshni parameters.

3.1.4 Strain impacts

Strain is an essential parameter, it affects the physical properties of the alloy. Recent electronic applications are gradually more integrating structures that are used on the nanoscale, such as optical devices based on quantum wells. As the chips are growing smaller, the strain effects appear as one material structure is adapting to another has a large impact on the device features [35].

In heterojunctions semiconductor materials, the lattice constant of one material is different from another one. This means it does not equivalent exactly to the second material and it constitutes the well and barrier lattice parameters which are different in the relaxed materials. In general, the heterojunctions thin films of one semiconductor are deposited on much thicker substrates of another [36]. This means if the well thin layer grows on thick barrier, the barrier will impose its lattice parameter in the well plane. Figure 3.2 shows the elastically growth of strained QW in tension and compression.

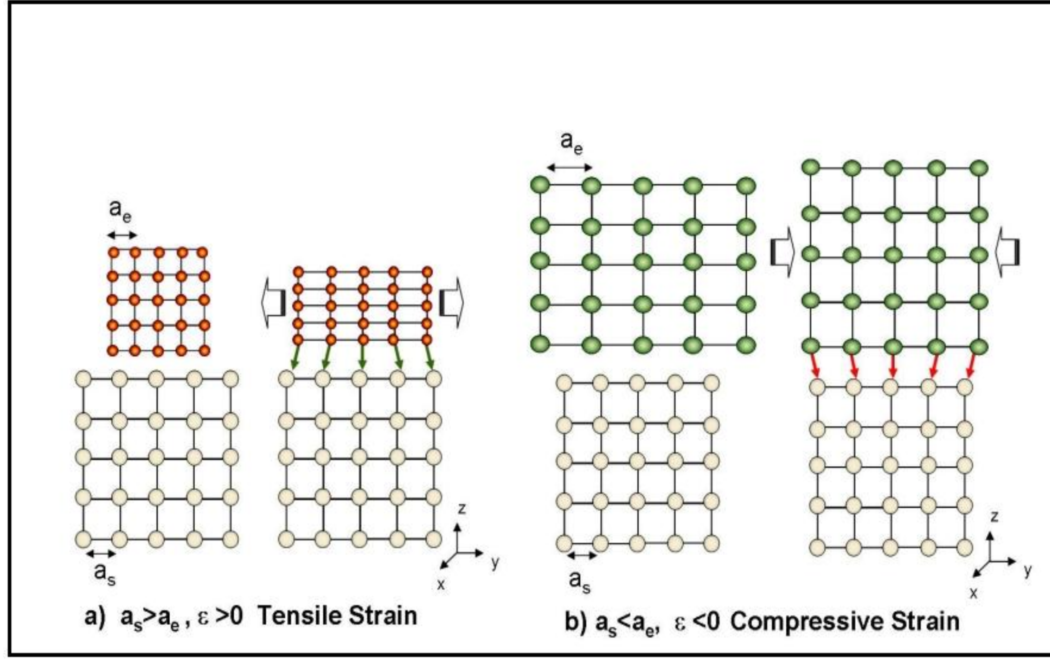

Figure 3.2 Elastically growth (a) tensile-strained and (b) compressively-strained layers grown on thick substrates [6].

Lattice constant of the epilayer material and substrate are presented as a_e and a_s, respectively. The layer plane strain $\varepsilon_{||}$ is given then by:

$$\varepsilon_{||} = \varepsilon_{xx} = \varepsilon_{yy} = \frac{a_s - a_e}{a_e} \tag{3.11}$$

According to the biaxial $\varepsilon_{||}$ stress, the layer relaxes along the growth direction in the plane of substrate, while the uniaxilaly strain $\varepsilon_{\perp}$ is strained in the perpendicular direction which is equal to the ε_{zz}. This has an opposite sign to that of the plane strain $\varepsilon_{||}$ as:

$$\varepsilon_{\perp} = -2\frac{\sigma}{1-\sigma} = \frac{2C_{12}}{C_{11}}\varepsilon_{||} \tag{3.12}$$

where C_{11} and C_{12} are elastic stiffness constants and σ is the Poisson's ratio.

The compressive strain occurs when $a_e < a_s$, $\varepsilon_{xx} = \varepsilon_{yy} < 0$, and, $\varepsilon_{zz} > 0$, whereas in tensile strain $a_e > a_s, \varepsilon_{xx} = \varepsilon_{zz} > 0$ and $\varepsilon_{zz} <.0$.

The total strain can be resolved into a purely axial component, ε_{ax}:

$$\varepsilon_{ax}= \varepsilon_{\perp} - \varepsilon_{||} \approx - 2\varepsilon_{||} \qquad (3.13)$$

and the hydrostatic constituent $\varepsilon_{vol}=\Delta V/V$

$$\varepsilon_{vol}=\varepsilon_{xx}+\varepsilon_{yy}+\varepsilon_{zz} \approx \varepsilon_{||} \qquad (3.14)$$

Strain induces a drastic modification in the band structure, which induced a change in the electronic properties with respect to the relaxed bulk semiconductor [6].

Figure 3.3 shows the properties of both compressive and tensile strained structures. In the compressive strain, the heavy and light hole splitting increases at k=0, while the effective mass of the heavy hole decreases in-plane direction. This causes a decrease of the hole density of state DOS which reduces the threshold current density. Moreover, the light-hole states, which do not participate in the lasing transition are more in energy from the heavy-hole states in compressively strained structures compared to that of the unstrained one. These states are thus fewer occupied, which leads to an increase laser efficiency of the semiconductor. One can also reveal that the differential gain is higher in a strained structure than in a lattice matched one [6].

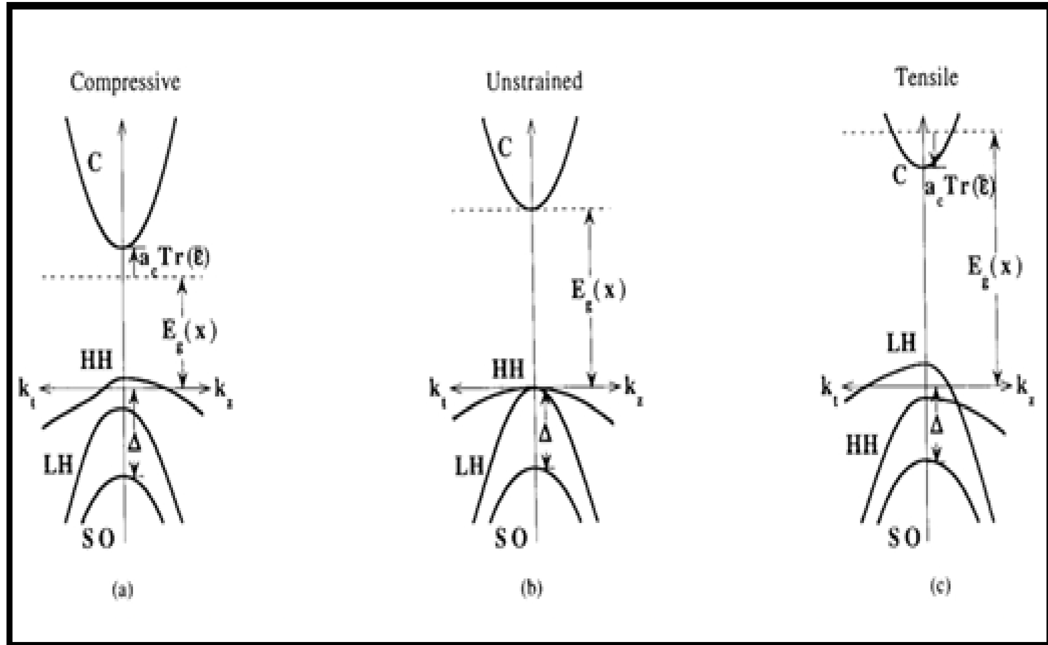

Figure 3.3: Schematic diagram showing the bulk band structure of three $In_{1-x}Ga_xAs$ ternary strained layers grown on InP substrate [6].

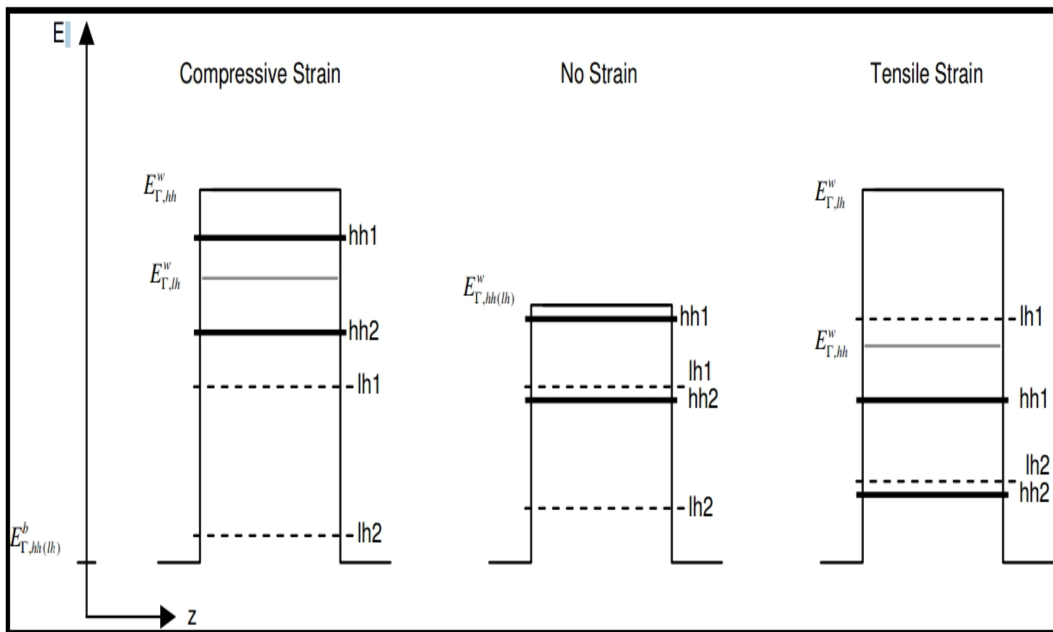

Figure 3.4: Diagram of the locations of confined states in strained and unstrained Quantum Well structures. In the right and left figures, only the well material is supposed to be strained. $E^{W}_{\Gamma,hh}$ is the bulk band edge of the well material [6].

Figure 3.3 illustrates the band structure in the k direction. The bulk bands are still parabolic with effective masses, in unstrained material and the effective masses can be expressed as:

$$m^{z}_{hh}=\frac{m_o}{\gamma_1-2\gamma_2} \quad (3.15)$$

$$m^{z}_{lh}=\frac{m_o}{\gamma_1+2\gamma_2} \quad (3.16)$$

In z-direction, the effective masses can be expressed as::

$$m^{z}_{hh}=\frac{m_o}{\gamma_1+\gamma_2} \quad (3.17)$$

$$m^{z}_{lh}=\frac{m_o}{\gamma_1-\gamma_2} \quad (3.18)$$

On $k_{x\text{-}y}$ plane, the advantages of strained quantum well are high-power pump laser and low threshold current operation.

The compressive strain is the most focused strain in both theoretical and experimental studies. The main reason for this is that the compressive strained QW have a reduced effective mass for the top heavy-hole subband in the plane of QW.

The density of state is reduced by the effective mass reduction and this lowers threshold carrier density. When the threshold carrier density is reduced, it causes a reduction in Auger recombination rate and threshold current density.

3.1.5 Model solid theory

Van de Walle and Martin suggested to calculate strain impacts on the band line-ups by model solid theory [37-38]. The most important parameters in the semiconductor are the band offset parameters, which has been used to design heterostructure electronic and optoelectronic devices. The relative band configuration of band edges between the QW and the barrier is the total band discontinuity which is distributed over the conduction and valence bands, as ΔE_c and ΔE_v. The band discrete relies on

the semiconductor and the quantity of mismatch strain at the interface. The quantum well structure, optical confinement factor and gain depend strongly on the band lineup of the heterostructure.

Figure 3.5 illustrates a simple schematic of band energy diagram for both of barrier and well structure. The energy of the potential barrier, ΔE_g is obtained from the variation between the bulk band gap energy of the barrier layers and the strained band gap energy of the active layer. The band offset ratio for conduction and valence band, $Q_{c,v}$, is found by discontinuity fractions of $\Delta E_{c,v}/\Delta E_g$.

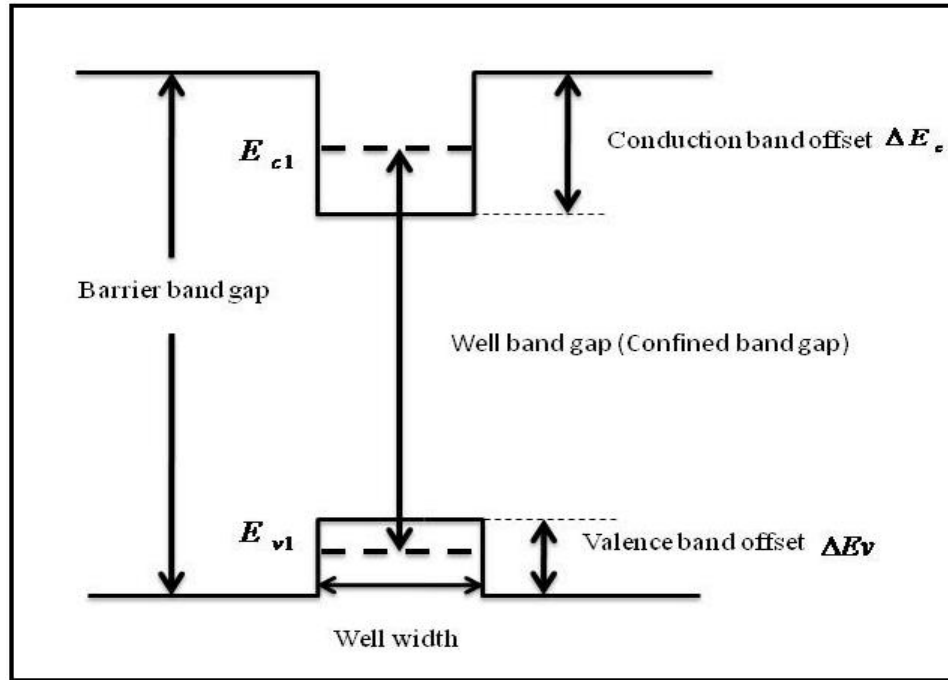

Figure 3.5: Schematic energy band line-up of quantum well structure.

The conduction band location can be determined by simply adding the strained band gap energy to the valence band position. The unstrained valence band edge of the active region material is set as the reference energy of zero. The valence band position is given by:

$$E_v(x,y) = \begin{cases} E_{v,av}(x,y) + \dfrac{\Delta_o(x,y)}{3} + \delta E_{hh}(x,y), & \text{for hh (compressive strain)} \\ E_{v,av}(x,y) + \dfrac{\Delta_o(x,y)}{3} + \delta E_{lh}(x,y), & \text{for lh (tensile strain)} \end{cases} \qquad (3.19)$$

where $E_{v,av}(x,y)$ is the average valence subband energy and Δ_o is the spin-orbit split-off band energy.

The conduction band is shifted by the energy $\delta E_c(x,y)$:

$$\delta Ec(x,y)=2a_c(1-\frac{C_{12}}{C11})\varepsilon \quad (3.20)$$

the valence bands are shifted by energy, $\delta E_{hh}(x,y)$ and $\delta E_{lh}(x,y)$ and are expressed as:

$$\delta E_{hh}(x,y)= -P_\epsilon - Q_\epsilon \quad (3.21)$$

$$\delta E_{lh}(x,y)= -P_\epsilon + Q_\epsilon \quad (3.22)$$

where P_ϵ and Q_ϵ is equal to:

$$P_\epsilon=-2|a_v|(1-\frac{C_{12}}{C_{11}})\varepsilon \quad (3.23)$$

$$Q_\epsilon = -b(1+2\frac{C_{12}}{C_{11}})\varepsilon \quad (3.24)$$

where a_c and a_v are the conduction and valence band hydrostatic deformation potentials, b is the valence band shear deformation potential, C_{11} and C_{12} are elastic stiffness constant.

The absolute value of hydrostatic deformation potential for valance band, a_v, is used to reconcile differing sign conventions found in literature [6]. The strained band gaps can then be expressed as:

$$E_{c\text{-}hh}(x,y)=E_g(x,y)+\delta E_c(x,y)-\delta E_{hh}(x,y) \quad (3.25)$$

$$E_{c\text{-}lh}(x,y)=E_g(x,y)+\delta E_c(x,y)-\delta E_{lh}(x,y) \quad (3.26)$$

The position of the conduction band is:

$$E_c(x,y)=\begin{cases} E_v(x,y)+\ \delta E_{c\text{-}hh}(x,y), & \text{for hh (compressive strain)} \\ E_v(x,y)+\delta E_{c\text{-}lh}(x,y), & \text{for lh (tensile strain)} \end{cases} \tag{3.27}$$

The conduction band offset is given by:

$$\frac{\Delta E_c}{\Delta E_g}=1-\frac{E_v^w-E_v^b}{E_g^b-E_g^w} \tag{3.28}$$

where E_v^w and E_v^b are the valence band positions in the well and barrier materials, respectively, and E_g^b and E_g^w are the strain modified band gaps ($E_{c\text{-}hh}$ for compressive strain and $E_{c\text{-}lh}$ for tensile strain) for the well and barrier materials. Figure 3.6 shows the band line-up of compressive, tensile strain and lattice matched.

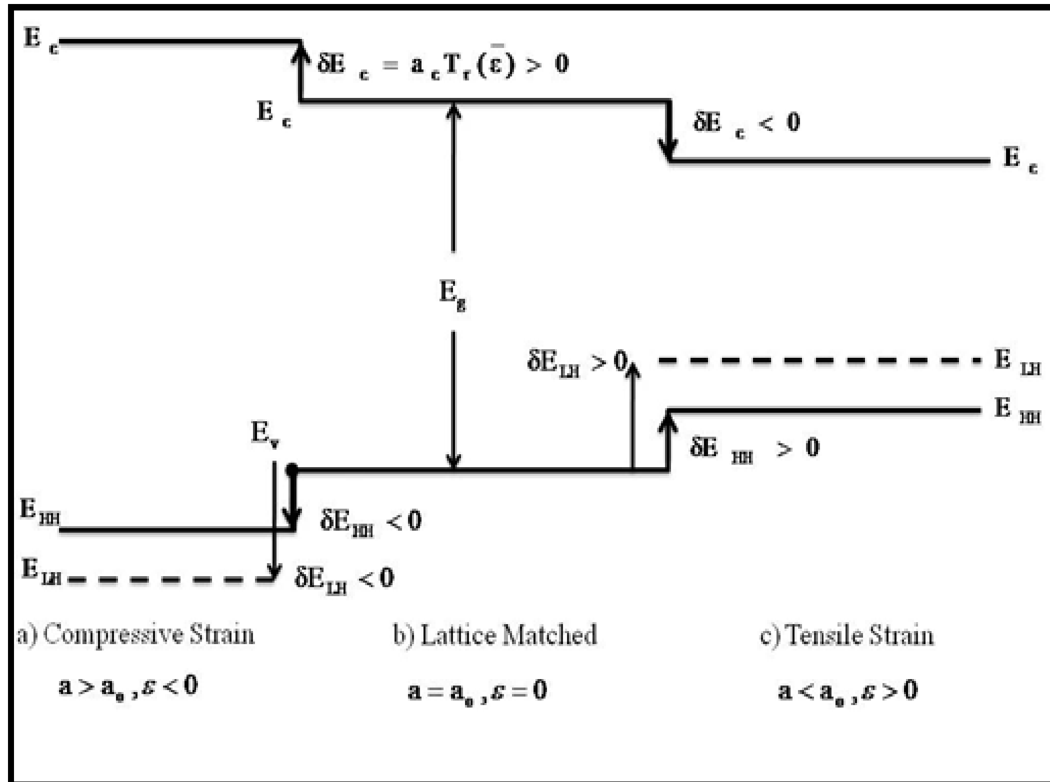

Figure 3.6: Band line-up of strained semiconductor (a) compressively strained, (b) lattice matched, and (c) tensiley strained layer.

3.1.6 The band anti-crossing model (BAC)

Nitrogen incorporation into the conventional III-V semiconductor creates a huge revolution in the optoelectronic device fabrication. It was exposed that substitution of group V elements with nitrogen leads to a remarkable change in the structural energy band of the group III-V semiconductors [9, 10, 11, 39].

This model considers the interaction of the localized N states with extended conduction-band state. The extended conduction states of matrix semiconductor and the N localized state are expressed as the energies of E_M and E_N, respectively.

The coupling between the two states is described by the following matrix equation:

$$\begin{vmatrix} E\text{-}E_M & V_{MN} \\ V_{MN} & E\text{-}E_N \end{vmatrix} = 0 \tag{3.29}$$

V_{MN} is the matrix element describing the coupling effect. At low N concentration in the group-V sublattice sites, the V_{MN} is equal to $C_{MN}\sqrt{x}$, where C_{MN} is a coupling constant and x is the N concentration in the III-N-V semiconductor alloy. An increase in the V_{MN} value with increasing N concentration leads to a strong repulsion between E_+ and E_-. The solution eigenvalue of Equation (3.29) gives us the dispersion relation for $GaN_xAs_yP_{1-x-y}$:

$$E_\pm = \frac{1}{2}\left[E_N + E_M \pm \sqrt{(E_N - E_M)^2 + 4V_{MN}^2}\right] \tag{3.30}$$

The big band gap bowing in GaAsN becomes apparent when N concentration increases. This feature as well as the band gap bowing was effectively explained with a simple phenomenological model, the so-called BAC model [39].

3.1.7 Electron effective mass

Effective masses of charged carriers are among the most significant essential parameters in a semiconductor. They have vital roles in quantum confinement energy, optical dipole matrix elements, band filling, carrier mobility, etc., and thus they play an important role in a broad range of electronic and optoelectronic applications.

The electron and hole effective masses are determined by the energy dispersion of their respective conduction and valence bands in the reciprocal lattice. Thus they provide a sensitive means of closely examining the electronic band structure of a semiconductor.

In dilute nitrides, the incorporation of N into conventional III–V semiconductors such as GaInAs band-gap has been found to introduce strikingly strong perturbation to the band structure of the host lattices, leading to a number of extraordinary effects, such as a giant band-gap bowing, a strong reduction in the pressure and temperature dependence of the band-gap energy [39].

The flattening of the $E_{\pm}$ curves for energies near E_N which is one of the most striking features of the BAC results, it refers to the large increase in the effective mass in both subbands. A strong non-parabolicity of the conduction band can also be described from Figure 3.10 for GaNAsP alloy according to the BAC model.

The electron effective mass is another important material parameters and depends strongly on the electron energy relative to localized E_N level.

The change in electron effective mass due to the nitrogen modified conduction band can be found by Skierbiszewski et al [22] as:

$$m^{*}=m_M\left[1+\left[\frac{V_{MN}}{E_N-E_-}\right]^2\right] \qquad (3.31)$$

where m_M is the electron effective mass in the parabolic of the semiconductor matrix. m_M is calculated by interpolation of constituent binaries.

The reduced band gap energy by adding N increases the electron effective mass. This case is unlike other conventional alloy semiconductors. It has a deep influence on the strength of the electron–electron and electron–phonon interactions and therefore on every feature of the performance (threshold current,etc.) of semiconductor lasers.

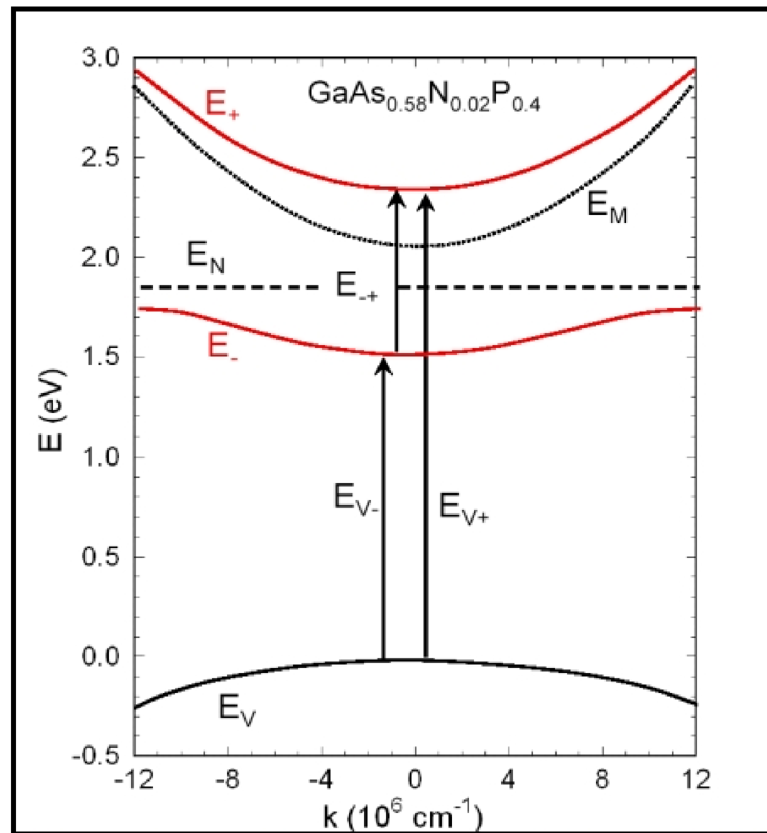

Figure 3.7: A schematic diagram of a $GaAs_{0.58}P_{0.4}N_{0.02}$ HMA illustrating the splitting of the original conduction band E_M into E_+ and E_- due to the interaction of the N level E_N with E_M [40].

CHAPTER 4

STRUCTURAL AND ELECTRONIC PROPERTIES of GaNAsP/GaP QUANTUM WELL

4.1. Binary Compounds GaAs and GaP

Gallium arsenide (GaAs) is a compound of the elements gallium and arsenic, it is a III-V semiconductor. GaAs is one of the most important technological and attractive compound semiconductor material [41]. It is also one of the commonly studied binary semiconductor material. The band structure parameters of GaAs are known with a better accuracy than for other compound semiconductors. Particular properties studied are its direct band gap for photonic applications [Jovanović1 et al., 2008], Nanotubes [Ghosh et al., 2007] and its internally-carrier transport and higher mobility for generating microwaves [Ng, 2002] [42]. The direct band gap property is the most important feature to fabricate QW; this feature helps the alloys to emit light efficiently in optoelectronic devices such as light emitting diodes (LEDs), solar cell (SC), detectors etc.

Another main binary material is Gallium phosphide and it has an indirect band gap. Therefore GaP is unsuitable as an efficient LED material. GaP is used in the fabrication of low-cost red, orange, and green light-emitting diodes (LEDs) with low to medium brightness since the 1960s. It has a comparatively short life at higher current and its lifetime is sensitive to temperature. Pure GaP LEDs emit green light at a wavelength of 555 nm. Nitrogen-doped GaP emits yellow-green (565 nm) light, zinc oxide doped GaP emits red (700 nm). Figure 4.1 shows the crystal structure of Zinc Blende of (ZB) GaAs and GaP.

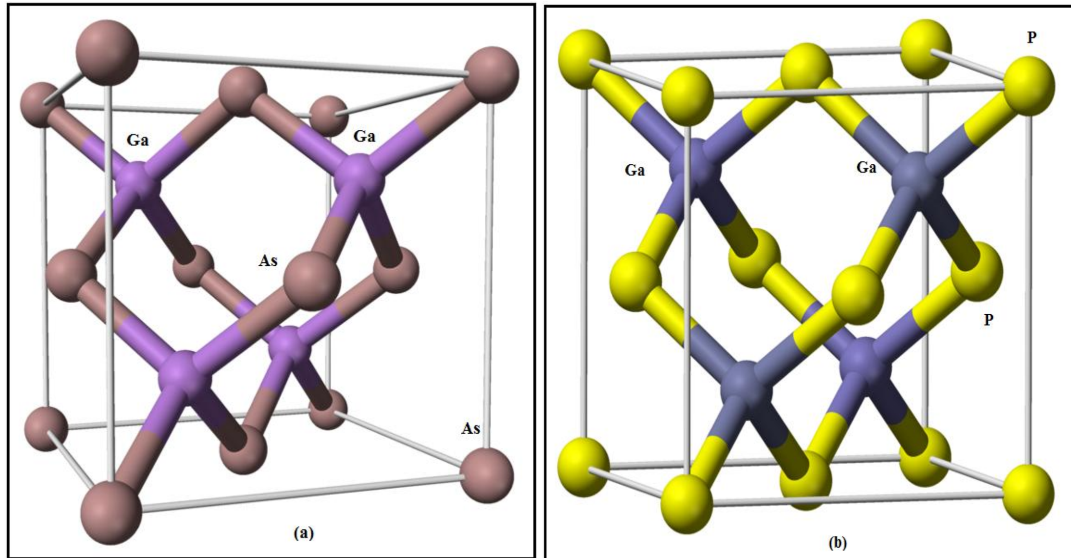

Figure 4.1: 3D crystal structure of zinc blende a) Gallium Arsenide, GaAs, and b) Gallium Phosphide, GaP [43,44].

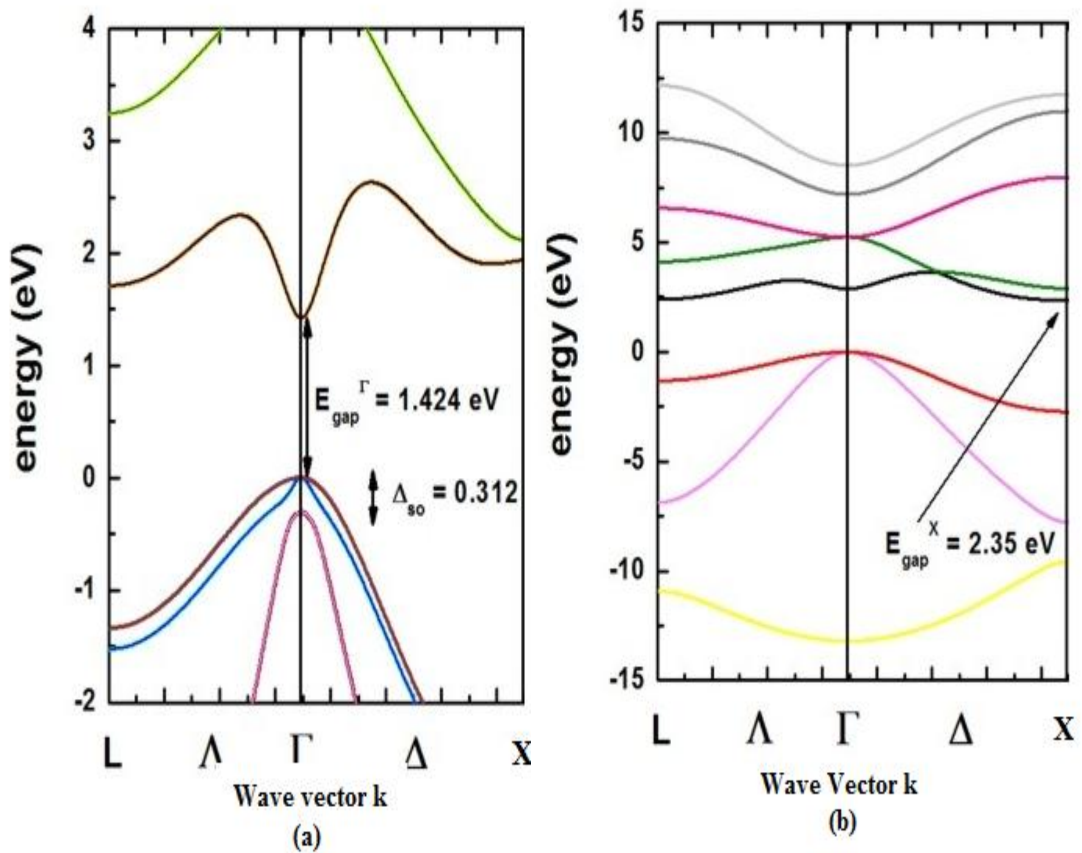

Figure 4.2: Band structure of a) GaAs and b) GaP , respectively [45].

4.2 Ternary Compounds $GaAs_{1-y}P_y$

$GaAs_{1-y}P_y$ was one of the initial material systems used for visible-spectrum LEDs (Holonyak and Bevacqua 1962). $GaAs_{1-y}P_y$ is a ternary compound based on GaAs and GaP [46]. Gallium arsenide is a direct gap semiconductor and gallium phosphide is an indirect semiconductor, when alloyed, there is a crossover point where $GaAs_{1-y}P_y$ will transform from being direct gap material to indirect gap material. GaAs substrates were already available, as phosphorus is added to GaAs, the ternary alloy $GaAs_{1-y}P_y$, or briefly GaAsP, is shaped. The addition of phosphorus increases the band gap of GaAs, which emits in the infrared at 870 nm. The visible wavelength range starts at about 750 nm, so that a small quantity of phosphorus is enough to reach visible-spectrum light emitters, this means red, yellow and orange colored LED can be made with $GaAs_{1-y}P_y$.GaAsP and GaP LEDs are commonly doped with isoelectronic impurities such as nitrogen [47].The isoelectronic impurities form an optically active level within the forbidden gap of the semiconductor so that carriers recombine radiatively using the nitrogen levels, which will be explained in the next section.

Figure 4.3 shows that $GaAs_{1-y}P_y$ is a direct-gap semiconductor for low phosphorus mole fractions. The direct–indirect intersection occurs at phosphorus mole fractions of about 45–50%; the $GaAs_{1-y}P_y$ becomes indirect and the radiative efficiency drops rapidly.

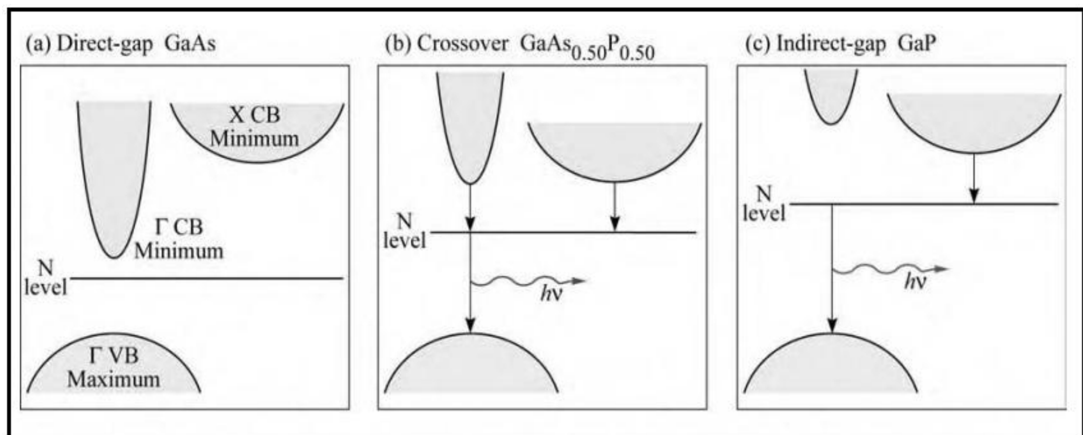

Figure 4.3: Schematic band structure of GaAs, $GaAs_{1-y}P_y$ and GaP, respectively [47].

Figure 4.4 shows the Γ and X intersection of $GaAs_{1-y}P_y$ at 50% P content, the direct-indirect intersect clearly emerges. The both direct and indirect energy increases by adding phosphorus into the system. On the other hand, the direct gap energy increases quicker with phosphorous composition than the indirect one. At x concentration of about 0.50, they crossover and the material goes from being a direct gap semiconductor to an indirect gap semiconductor.

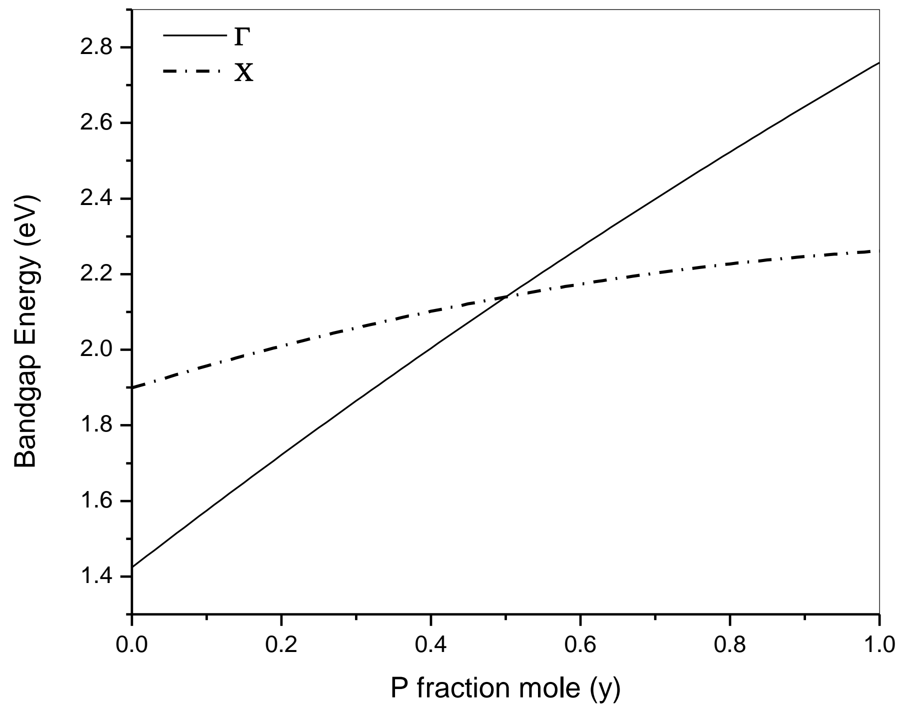

Figure 4.4: Calculated energy positions of the Γ (solid line) and X (dashed line) conduction bands of the $GaAs_{1-y}P_y$ alloy system, direct-indirect crossover occurs at 0.5% P composition.

4.3 Quaternary Compound $GaN_xAs_yP_{1-x-y}$

The implantation of N in amalgamation with As allows for the required modification of the lattice constant of the quaternary material system GaNAsP to GaP-substrate. A novel As-rich dilute nitride material system used and named as a $GaN_xAs_yP_{1-x-y}$ [3].

Nowadays $GaN_xAs_yP_{1-x-y}$ is one of the quaternary materials studied and focused by the researchers. Compressively strained GaNAsP multiquantum well heterostructure (MQWHs) was grown pseudomorphically on GaP-substrates [3] by MOVPE without

any formation of misfit dislocation. The material growth of high quality films on GaP-substrate creates a direct band structure and high luminescence efficiency. This category of the nitride semiconductor alloy system has a great potential function in silicon photonics. This novel semiconductor alloy is shown to have a direct band structure and it can be grown without the configuration of extended defects on GaP (lattice-matched) and for this reason on silicon substrates (GaP has a similar lattice constant of silicon).

Prof. Hiroo Yonezu and co-workers of the University of Toyohashi in Japan [48] demonstrated the heteroepitaxial growth of Ga(NP)/GaP layer sequences on silicon-substrates with high structural precision without the creation of any misfit dislocations and antiphase domains.

This unique position of silicon (Si) is based on several major advantages over other semiconductors:

I. It is widely available and simple to purify.
II. It is easy to handle and to manufacture.
III. It has good thermal and mechanical properties.
IV. In combination with silicon oxide there are further advantages for chip processing techniques (diffusion barrier, surface passivation, insulator, etc.).

The indirect GaP semiconductor has a lattice constant nearly equal to that of Si has been shown in Figure 4.5. Therefore, the binary material system GaP (gallium phosphide) and $GaN_xAs_yP_{1-x-y}$ can be grown lattice matched to Si-substrate.

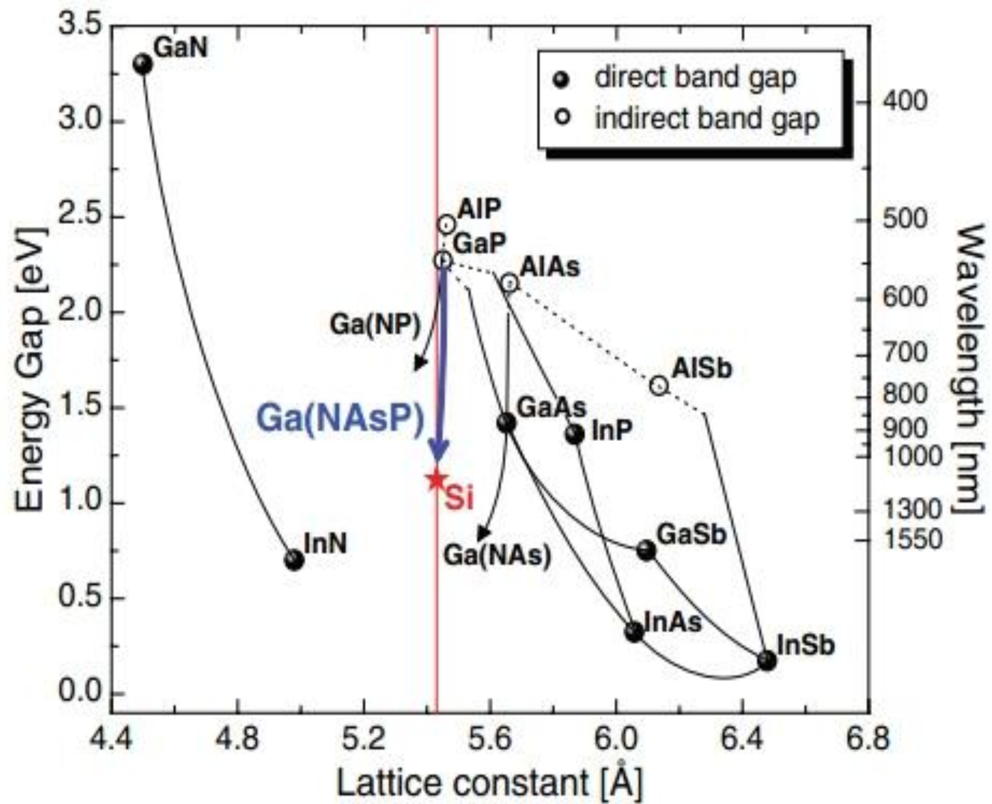

Figure 4.5:.Energy gap versus the lattice constant of the most common III–V semi-conductors in comparison to Si [3].

4.4 Model Calculations of $GaN_xAs_yP_{1-x-y}$/GaP

In this section, $GaN_xAs_yP_{1-x-y}$/GaP material system under hydrostatic pressure will be revealed some structural and electrical properties such as band gap energy, effective mass and AR recombination and how it was changing according to the N mole fraction amount in the band structure or the system. First some calculated data has been reviewed without hydrostatic pressure.

4.4.1 Material parameters of $GaN_xAs_yP_{1-x-y}$ QW

The material parameters except for the band gap energies of $GaN_xAs_yP_{1-x-y}$ laser systems are linearly interpolated from those of the binary materials [27] and they are tabulated in Table 3.1. For example, a lattice constant interpolation scheme of the quaternary material $GaN_xAs_yP_{1-x-y}$ is:

$$a_{GaNAsP}=\frac{xya_{ABD}(u)+y(1\text{-}x\text{-}y)a_{BCD}(v)+x(1\text{-}x\text{-}y)a_{ACD}(w)]}{xy+y(1\text{-}x\text{-}y)+x(1\text{-}x\text{-}y)} \tag{4.1}$$

where

$$u=\frac{1\text{-}x\text{-}y}{2},\qquad v=\frac{2\text{-}x\text{-}2y}{2},\qquad w=\frac{2\text{-}2x\text{-}y}{2}$$

where x is the N mole fraction, y mole fraction of As in $GaN_xAs_yP_{1-x-y.}$

4.4.2 Parameters within BAC model for $GaN_xAs_yP_{1-x-y}$ QW

The GaNAsP material can be modelled by using GaN, GaAs, and GaP binaries. The GaN has a larger band gap energy (~3.3 eV for ZB) according to GaP and GaAs. Thus the introduction of As reduces the GaN_xAs_{1-x} band gap.

In order to reproduce the band structure of real semiconductor's as correctly as possible, the interaction matrix element V_{MN} and the N level E_N must be determined along with their dependence on concentration in band anti-crossing model. As a result, an exact form for the effective mass of electron is required for the measurement of different laser parameters [6].

The energy of the GaAsP matrix conduction band is E_M and with its bowing parameters is given as [6]:

$$E_M = yE_{oGaAs} + (1\text{-}y)E_{oGaP} + y(1\text{-}y)C_{GaAsP} - (\,3.5)x \tag{4.2}$$

where x and y denote the N and As concentrations, respectively. C_{GaAsP} is the GaAsP bowing parameter being equal to (-0.19) eV [27].

The nitrogen energy level E_N is obtained from the N energy level of both the GaAsN equal to 1.67 eV and GaPN equal to 2.18 eV [3] as:

$$E_N = (y)1.67 + (1-x-y)2.18 \quad (4.3)$$

The strength of the Γ-E_N interaction is described by the matrix element V_{MN} [8]. V^2_{MN} is the square of the matrix element depends on the mole fraction of nitrogen atom as:

$$V_{MN} = C_{MN}\sqrt{x} \quad (4.4)$$

where the interaction parameter C_{MN} is 1.9 eV and x is N concentration. By substituting all these values into the dispersion relation equation, the subbands (transition) energies E_- and E_+ will be determined as:

$$E_{\pm} = \frac{1}{2}\left[E_N + E_M \pm \sqrt{(E_N - E_M)^2 + 4V^2_{MN}}\right] \quad (4.5)$$

Figure (4.6) shows that the lower subband energy E_- shifts towards lower energies with nitrogen concentration of $GaN_xAs_yP_{1-x-y}/GaP$. On the other hand, the higher energy E_+ shifts towards higher energies with nitrogen concentration. The energy difference between E_- and E_+ strongly depends on the N concentration; the separation increases almost linearly with x in the calculated concentration range.

It is seen from figure 4.7 that strain is compressive and it decreases with increasing nitrogen concentration. The compressive strain widens the semiconductor band gap, while it will diminish under a tensile hydrostatic stress is [51]. This decrease in compressive strain is important, which is another factor to manufacture the long wave length device.

The strain in the same material will be different according to the variations of As concentration because of the physical properties of both N and As as mentioned previously. These properties related to the electronegativity and atomic radii for both elements. Figure 4.8 shows that the magnitude of the compressive in well increases with increasing As concentration.

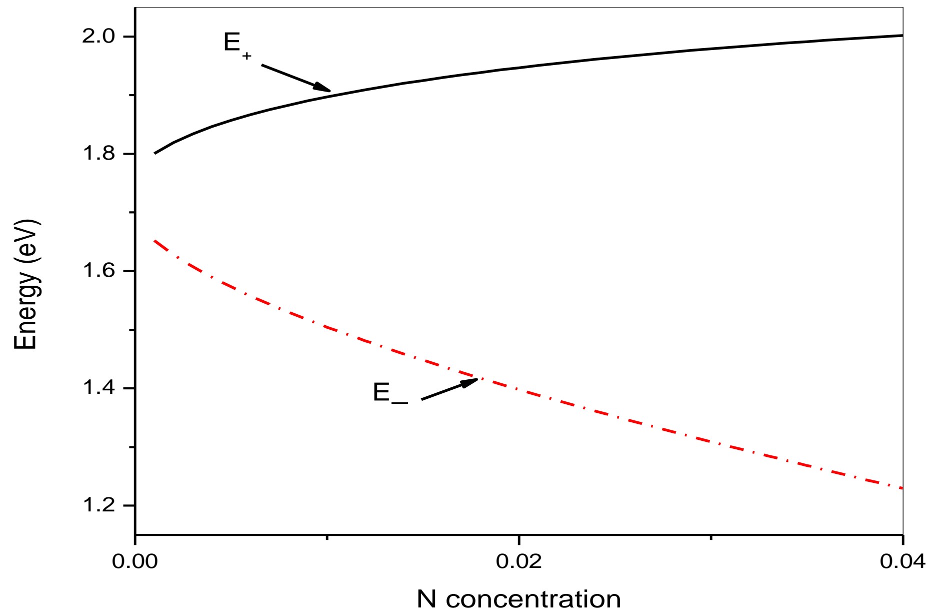

Figure 4.6: Calculated subband energies E_- and E_+ versus nitrogen concentration for $GaN_xAs_yP_{1-x-y}$ on GaP substrate according to BAC model. The difference between E_- and E_+ energies strongly depends on the N composition, the splitting up increases approximately linearly with x in the calculated concentration range.

Figure 4.7 illustrates the calculated variation of the strain as a function of nitrogen concentration.

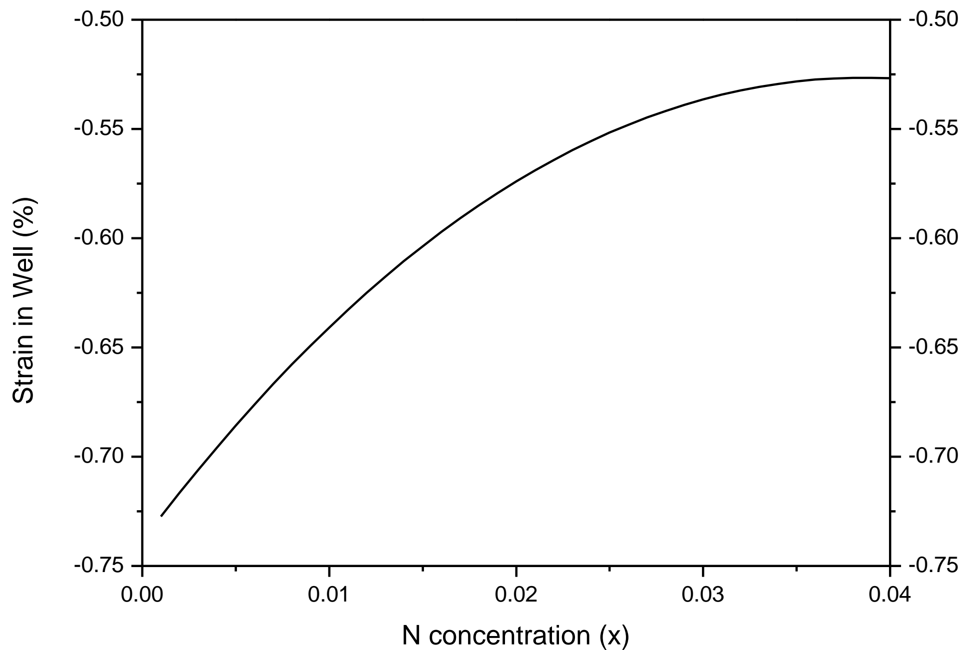

Figure 4.7: The calculated strain in well with respect to the nitrogen concentration in $GaN_xAs_{0.8}P_{0.2-x}$/GaP QW.

It is seen from figure 4.7 that strain is compressive and it decreases with increasing nitrogen concentration. The compressive strain widens the semiconductor band gap, while it will diminish under a tensile hydrostatic stress is [51]. This decrease in compressive strain is important, which is another factor to manufacture the long wave length device.

The strain in the same material will be different according to the variations of As concentration because of the physical properties of both N and As as mentioned previously. These properties related to the electronegativity and atomic radii for both elements. Figure 4.8 shows that the magnitude of the compressive in well increases with increasing As concentration.

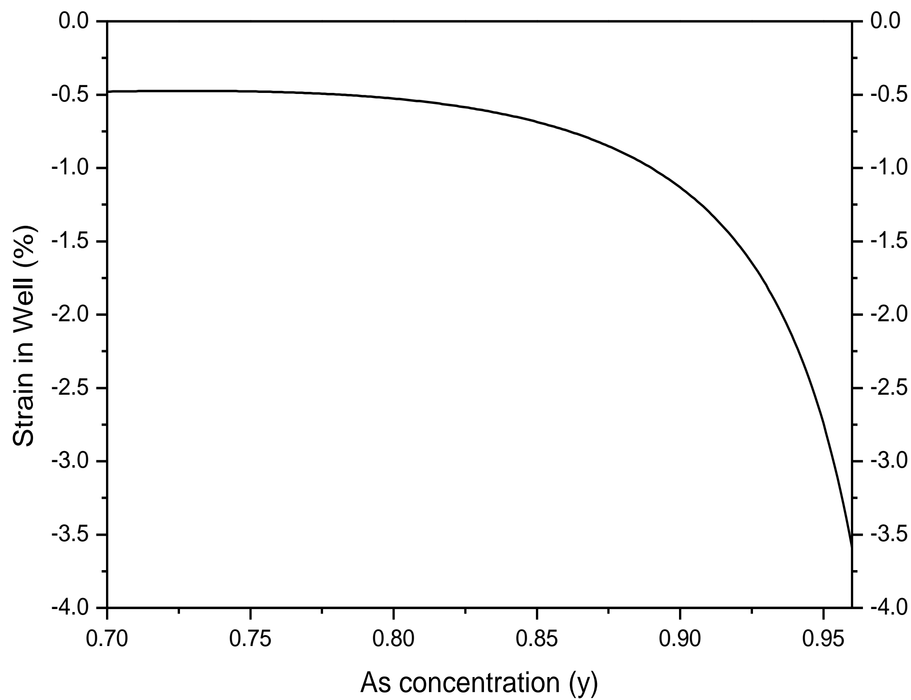

Figure 4.8: The strain in well as a function of As in $GaN_xAs_yP_{1-x-y}$/GaP QW

We want to illustrate in Figure 4.9 that the presence of strain narrows the energy gap.

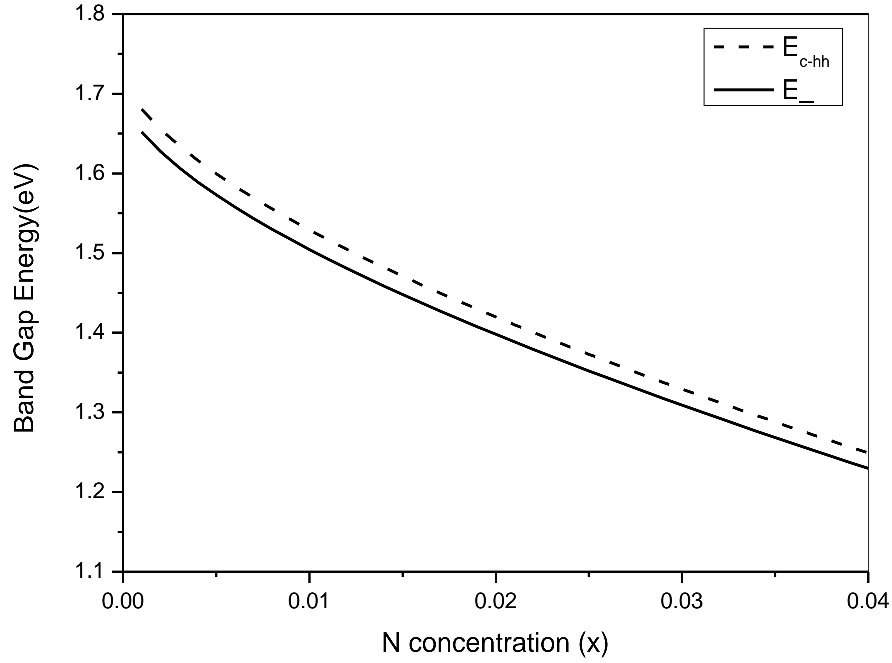

Figure 4.9: Band gap energy versus N concentration. $E_{c\text{-}hh}$ is the strained energy and E_- is the lowest subband according to band anti-crossing model.

4.4.3 Conduction band electron effective mass and N content

Novel material system, unlike other conventional alloy semiconductor, the effective mass of electron is proportional to the band gap. The N induced non-parabolicity of the effective mass of electron shows uncommonly large values. Large values of effective mass explain the large values of the conduction band density of states [3]. Since the density of state (DOS) is larger with increasing nitrogen fraction mole, the electron Fermi level moves gradually with injected carriers.

The coupling between the bottom of the conduction band and the N-induced levels adjusts the electron mass [17]. Figure 4.10 shows the variation of the effective mass of the conduction band as a function of N concentration.

This variation of the electron effective mass has been calculated by increasing nitrogen concentration using Eqn. (4.5) and Eqn. (3.31) for $GaN_xAs_{0.8}P_{0.2-x}$ on the GaP substrate system.

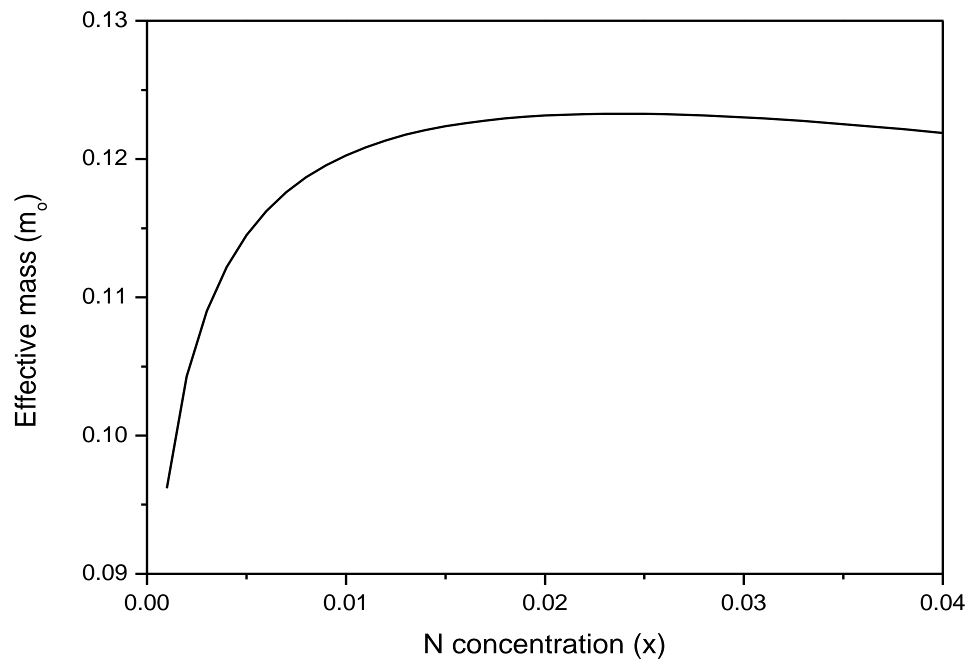

Figure 4.10: Electron effective mass of conduction band as a function of nitrogen concentration.

CHAPTER 5

INVESTIGATION OF THE NITROGEN DEPENDENCE OF THE NON-RADIATIVE LOSS MECHANISMS IN $GaN_xAs_yP_{1-x-y}$/GaP

5.1 Introduction

The loss mechanisms affect the performance of optoelectronic devices, especially laser device. The material loss processes are generally divided into spontaneous emission, carrier recombination at defect states and Auger recombination. The defect losses are insignificant if one is dealing with high-quality materials. The radiative and Auger losses are calculated microscopically [49]. Auger recombination (AR) is a process, named after the 20th-century French physicist Pierre-Victor Auger that involves the interaction of an electron and a hole with another carrier, all without the emission of light. Materials with small band gap tend to have a much higher Auger recombination. High Auger recombination in the band structure leads to non-radiative loss mechanism in the laser [50].

5.2 Types of non-radiative Auger recombination process

Auger recombination is a non-radiative recombination method when electrons and holes recombine across the energy gap, with the energy released exciting a third carrier either an electron higher into the conduction band or a hole into the valence band. There are two possible AR mechanism, band to band (direct Auger process) and phonon-assisted, both have been widely investigated for both bulk and quantum well semiconductor.

5.2.1 Direct Auger process

The two major direct and phonon-assisted CHCC and CHSH Auger recombination (AR) processes are shown in Figure 5.1.

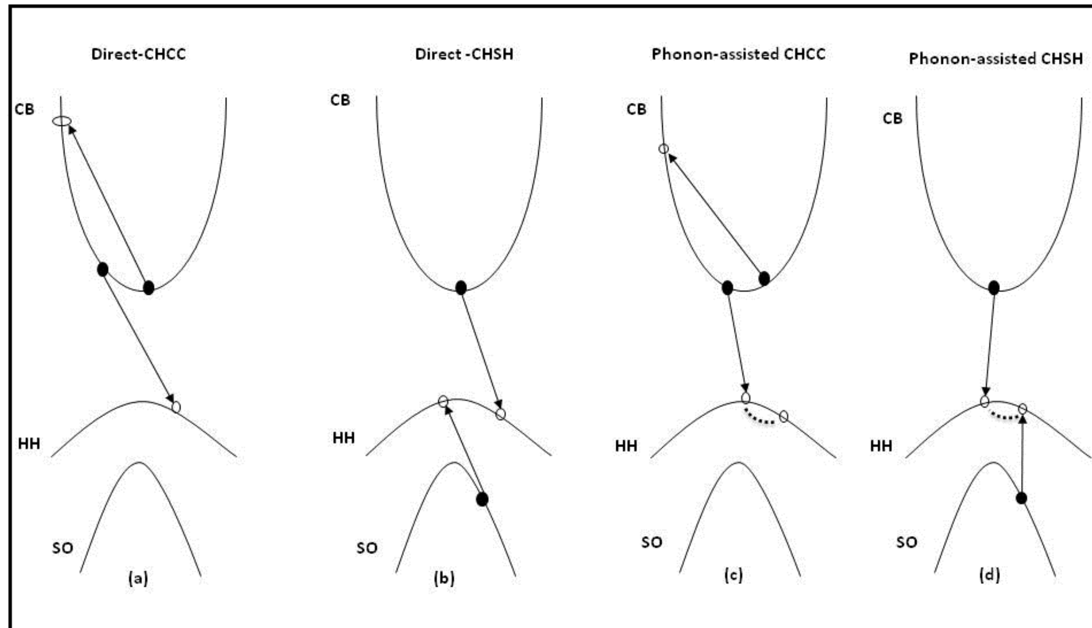

Figure 5.1: Schematic diagram of Auger recombination process.

In Figure 5.1, the electron in the CB recombine with a hole in the heavy hole band transferring its energy and momentum to an electron in the conduction band which is lifted to a higher state (CHCC), or an electron in the split-off band to an empty heavy hole state. The electron is represented by closed circles and holes by open circles. The arrow indicates the electron transitions. Symbols C, H and S designate conduction, heavy and split-off band, respectively.

Figure 5.2 shows both of CHCC and CHSH AR in QW laser semiconductor.

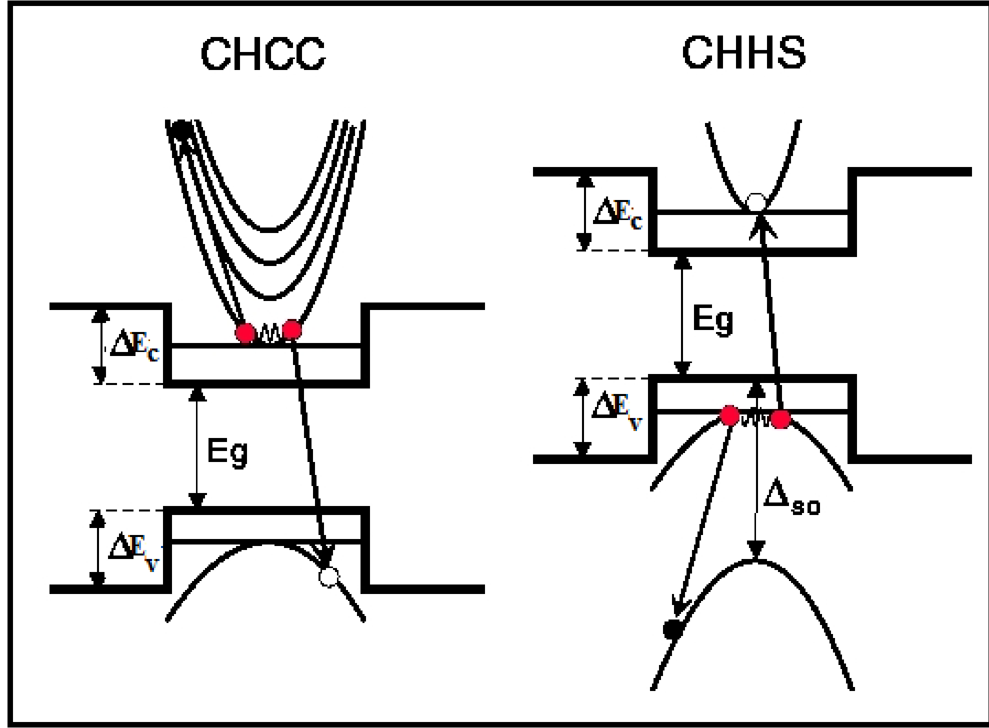

Figure 5.2: CHCC and CHHS Auger processes in a quantum well [51].

The direct Auger recombination rate can be expressed as:

$$C_d = C_o e^{-E_a/K_B T} \tag{5.1}$$

where E_a is the activation energy.

Assuming parabolic conduction, valence and spin-orbit bands and Boltzmann statistic minimum, activation energy E_a and the coefficient C_o for the CHCC direct Auger process can be written as:

$$E_a(CHCC) = \frac{m_c E_g}{m_c + m_{hh}} \tag{5.2}$$

$$C_o(CHCC) = \frac{4\pi}{\hbar} \frac{e^4 m_c (m_{hh} + m_c) |M_{ee}|^2}{E^2 (2m_{hh} + m_c)^2 k_B T} \tag{5.3}$$

where m_c and m_{hh} are the conduction band electron and valence band heavy-hole mass, respectively, and E_g is the band gap energy. $|M_{ee}|$ is the matrix element of the electron-electron interaction which can be taken for the CHCC process as:

$$|M_{ee}|^2=\left(\frac{\hbar^2}{2m_o}\right)^2\frac{m_o}{m_c}\frac{E_p}{E_g^3} \tag{5.4}$$

substituting Eqns.(5.2), (5.3) and (5.4) into the Eqn.(5.1), the direct Auger recombination rate for the CHCC Auger process becomes:

$$C_d(CHCC)\propto\frac{m_o(m_{hh}+m_c)}{(2m_{hh}+m_c)^2}\frac{1}{E_g^3}exp\left(-\frac{m_c}{m_c+m_{hh}}\frac{E_g}{k_BT}\right) \tag{5.5}$$

Similarly, the activation energy and coefficient C_o can written for direct Auger process CHSH as:

$$E_a(CHSH)=\frac{m_s(E_g-\Delta)}{(2m_{hh}+m_c-m_s)} \tag{5.6}$$

$$C_o(CHSH)=\frac{4\pi e^4}{\hbar}\left(\frac{m_{hh}}{m_v}\right)^2\frac{m_s(2m_{hh}+m_c-m_s)}{(2m_{hh}+m_c)^2}|M_{ee}|^2 \tag{5.7}$$

with the matrix element for the electron-electron interaction in the CHSH process given by:

$$|M_{ee}|^2=\left(\frac{\hbar^2}{2m_o}\right)^2\frac{f_{CH}f_{SH}}{E_g\Delta} \tag{5.8}$$

where f_{CH} and f_{SH} are oscillator strengths which can be represented in the Kane model by [7]:

$$f_{CH}=\frac{E_p}{3E_g}\ ,\qquad f_{SH}=\frac{E_p}{3\Delta\left(E_g+\Delta\right)}\frac{\hbar^2k_2^2}{2m_o}\left(1+\frac{m_s}{m_o}\right) \tag{5.9}$$

where E_p is the energy equivalent of the momentum matrix element, which is evaluated for different semiconductor by Lawaetz [7]. Here k_2 is the solution of

$$E_g\text{-}\Delta\text{-}E_s(k_2) = 0 \qquad (5.10)$$

Thus $|M_{ee}|^2$ gives as:

$$|M_{ee}|^2=\left(\frac{\hbar^2}{2m_o}\right)^2 \frac{E_p^2}{9E_g\Delta(E_g+\Delta)} \qquad (5.11)$$

The direct CHSH Auger rate can be found by inserting Eqns. (5.11), (5.10), (5.9), (5.8), (5.7) and (5.6) into Eqn.(5.1)

$$\begin{aligned} C_d(CHSH) \propto \left(\frac{m_{hh}}{m_v}\right)^2 \frac{m_s(2m_{hh}+m_c\text{-}m_s)}{(2m_{hh}+m_c)^2} \frac{1}{E_g\Delta^2(E_g+\Delta)} \times \\ exp\left(-\frac{m_s}{2m_{hh}+m_c\text{-}m_s}\frac{E_g\text{-}\Delta}{k_BT}\right) \end{aligned} \qquad (5.12)$$

where m_s is the mass of the spin-split-off band, Δ the spin-split of energy and m_v=(m_{hh}+m_{lh}) .

It is clear from the above equations that the relative strengths of these processes are heavily dependent on the band gap and effective masses.

5.2.2 Phonon-assisted Auger processes

The strong band structure dependence of the direct Auger processes arises from the conservation laws of energy and momentum. In the phonon-assisted Auger processes conservation of momentum can be fulfilled by the phonon (see Figure 5.1).

As a consequence, one may expect that the impact of the band structure is less important in phonon-assisted Auger processes.

The phonon-assisted AR rate is given by Huge [7] as:

$$C_p = \frac{A}{2\hbar^2}\left(\frac{4\pi e^2}{\varepsilon}\right)^2 m_{hh}\bar{\mu}\ \frac{|M_{ep}|^2|M_{ee}|^2}{e^{\hbar\omega/k_BT}-1}\left[\left[\frac{1}{(\bar{\mu}\,\overline{E_g}+\hbar\omega)^2}+\frac{e^{\hbar\omega/k_BT}}{(\bar{\mu}\,\overline{E_g}-\hbar\omega)^2}\right]\right] \tag{5.13}$$

with

$$\overline{E_g}=E_g\ ,\ \ \bar{\mu}=\frac{m_c}{m_{hh}} \tag{5.14}$$

For the CHCC process

$$\overline{E_g}=E_g-\Delta,\ \ \bar{\mu}=\frac{m_s}{m_{hh}} \tag{5.15}$$

For the CHSH process, A is the area of the QW, $\bar{\mu}E_g$ is the kinetic energy associated with the forbidden intermediate state, and $\hbar\omega$ is the phonon energy. In addition to electron-electron interaction M_{ee}, in this case the electron-phonon interaction M_{ep} is involved and this is described by [52]:

$$|M_{ep}|^2=\frac{\Omega_o}{AL_z}\frac{D^2}{2M\upsilon_s^2} \tag{5.16}$$

where D is the deformation potential, υ_s is the velocity of the sound and M is the sum of the masses of the atoms in the elementary cell of volume Ω_o. The element of the electron-electron interaction $|M_{ee}|$ is given by Eqn.(5.4) and Eqn. (5.8) for the CHCC and CHSH Auger processes respectively.

Substituting Eqns. (5.14), (5.16) and (5.4) into Eqn.(5.13) gives:

$$C_p(CHCC)\ \alpha\ m_o\left(\frac{m_{hh}}{m_c}\right)^2\left(\frac{1}{E_g^5}\right) \tag{5.17}$$

Similarly substituting Eqns. (5.15), (5.16) and (5.11) into Eqn. (5.13) yields

$$C_p(CHCC)\ \alpha\ \frac{m_{hh}^2}{m_s}\frac{1}{E_g\Delta^2(E_g+\Delta)(E_g-\Delta)^2} \tag{5.18}$$

5.3 Results and Conclusions

We have used these equations to calculate the Auger recombination process for both direct and phonon-assisted for III-N-V semiconductor $GaN_xAs_yP_{1-x-y}$/GaP QW as a function of the N mole fraction in the band structure. Figure 5.3 shows the calculated results. These results indicate that the increase in nitrogen concentration in $GaN_xAs_yP_{1-x-y}$ alloy causes a rapid increase in Auger recombination, especially in direct and phonon-assisted CHSH processes. This is a disadvantage for the laser, which reducing the efficiency and performance of the device.

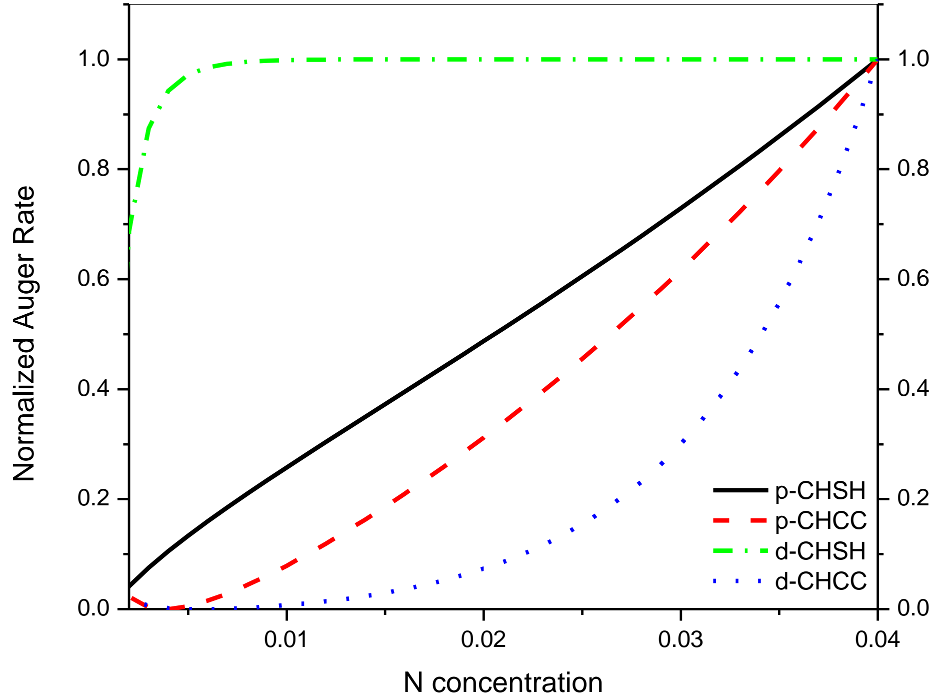

Figure 5.3: The normalized Auger rate as a function of N concentration for four types of Auger recombination processes for $GaN_xAs_{0.8}P_{0.2-x}$.

CHAPTER 6

ANALYSIS OF THE PRESSURE DEPENDENCE OF BAND STRUCTURE AND AUGER LOSSES IN $GaN_xAs_{0.8}P_{0.2-x}$/GaP QW

6.1 Introduction

Hydrostatic pressure, as it mentioned before in the introduction, provides a convenient system to vary continuously the band structure of semiconductor lasers, and hence to study systematically the internal electronics and optoelectronic process occurring. These include for example, loss mechanism such as Auger recombination, which is responsible for increasing the temperature (with intervalence band absorption loss mechanism) in the bulk 1.3-1.5 µm wavelength devices [8].

Shan et al. [15] found that the N incorporation into InGaAs alloys caused a strong interaction between a narrow resonant band formed by the N states and the conduction band due to the highly localized nature of the perturbation introduced by N atoms. This incorporation leads to dividing the conduction band and a reduction of the fundamental band gap. These are clearly explained in chapter 3. Shan related these changes in the optical transitions associated with the two conduction subband energy of the split lowest conduction band with variation In and N concentration and feature anti-crossing behaviour of the two conduction subband energy under pressure application. While Klar et al. showed that under pressure, the conduction band edge is shifted to higher energies rapidly [2], so the re-emerges into the gap. This reflects the low pressure coefficient of the cluster state, due to their weak hybridization with the perturbation host state. Another important element of the band structure parameters is the external perturbations such as temperature and pressure. Band gap energy and effective mass are strongly dependent on pressure.

6.2 Pressure Dependence of Parameters

The most important semiconductor properties rely on the analysis of band structure parameters. The band structure parameters depend on external perturbation such as temperature and pressure. The aim of this chapter is to investigate the pressure dependences of the band structures parameters such as strained band gap energy, effective mass and non-radiative Auger recombination processes for strained $GaN_xAs_yP_{1-x-y}/GaP$ laser structure.

6.3 Results and Conclusions

6.3.1 Analysis of BAC model with pressure in $GaN_xAs_{0.8}P_{0.2-x}/GaP$

The selected $GaN_xAs_yP_{1-x-y}/GaP$ QW band structure calculation depends on the dispersion relation. The influence of hydrostatic pressure on the band gap energy is determined as:

$$E_{\pm}=\frac{1}{2}\left[E_N+E_M(p)\pm\sqrt{(E_N-E_M(p))^2+4V_{MN}^2}\right] \quad (6.1)$$

here, $E_M(p)$ is the host material (GaAsP) pressure dependent conduction band edge, E_N is the energy level of the localized N state.

The pressure dependence of the conduction band is given as:

$$E_o(p)=E_o(0)+a(p)+bp^2 \ \ (eV) \quad (6.2)$$

where the constants a and b are the linear and non-linear pressure coefficients, respectively. Table (6.1) shows the pressure coefficients of direct band gap binary materials.

Table 6.1: Linear and non-linear pressure coefficients of *a* and *b* [53].

Material	a ($x10^{-2}$ eV/GPa)	b ($x10^{-4}$ eV^2/GPa^2)
GaN	39.0	-0.32
GaAs	10.8 ± 0.3	-14 ± 2
GaP	9.7 ± 0.8	-35 ± 6

The calculated pressure dependence of the energy for $GaN_xAs_{0.8}P_{0.2-x}$ QW lasers has been shown in Figure 6.1. It shows the pressure dependence of GaAsP (host matrix) energy (E_M) by using Eqn.(6.2). The nitrogen level location was obtained by interpolation of isolated N level (E_N) in GaP and GaAs [15] and assumed negligible vary with pressure.

The variation in lasing energy (E_-) with pressure can be calculated using the BAC model. The hydrostatic pressure calculations were used from the beginning as a critical investigation of the BAC model, because the nitrogen level E_N and the conduction band edge E_M shift at different rates under hydrostatic pressure, allowing one to continuously tune the repulsion effects between the energy states [15].

Hydrostatic pressure calculation can also be used to investigate to reveal the weakness or strength of the BAC model in the nitride III-V semiconductor alloys [20].

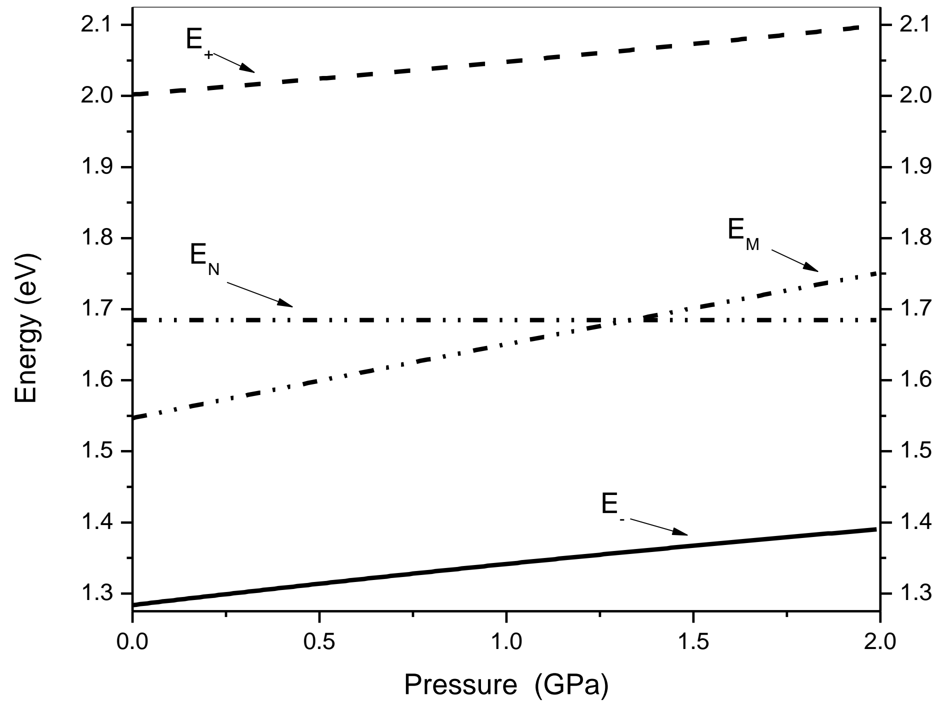

Figure 6.1: Pressure dependence of the energy for $GaN_{0.04}As_{0.8}P_{0.2-x}$ QW lasers. The pressure dependence of the GaAsP conduction band (E_M) is also shown.

We have shown in Figure 6.1 the calculated pressure dependences of E_+, E_-, E_N and E_M using BAC model. As it is seen from Figure 6.1 all these energies vary at different rates with pressure. Figure 6.2 illustrates a schematic variation of the related energies at three different pressure values. It is clearly shown in the Figure 6.2 that the hydrostatic pressure has the strongest impact on the lower subband (E_-) that narrows drastically at high pressure. Narrowing [15] of the band indicates a gradual, hydrostatic pressure-induced transformation in the nature of the lowest subband from an extended to highly-localized state, while the energy of nitrogen level E_N is insensible to applied pressure [10]. This transformation can be also shown as a pressure-induced enhancement of the effective mass and the DOS in the lower subband.

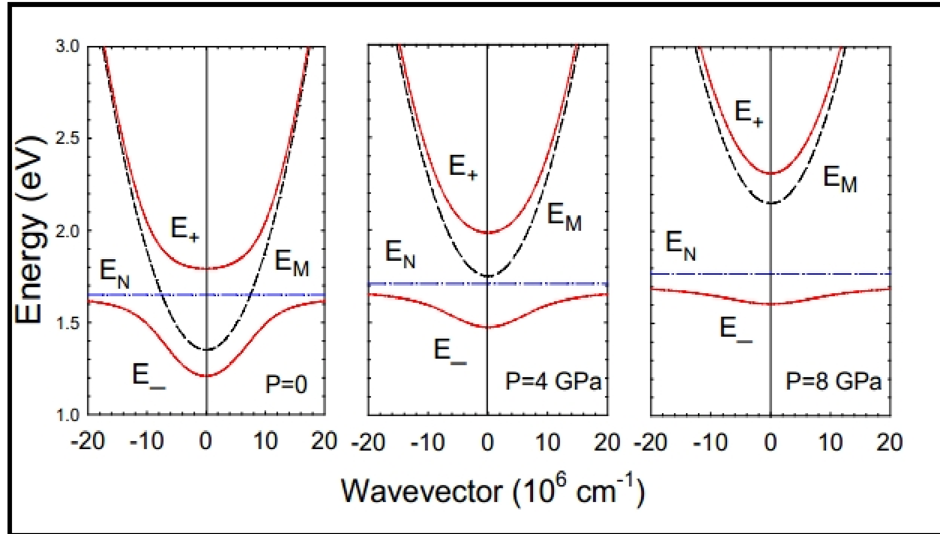

Figure 6.2: The calculated dispersion of the E_- and E_+ subbands at three different pressures [15].

6.3.2 Hydrostatic pressure dependence of strained band gap

The calculated strained band gap energy of $GaN_xAs_{0.8}P_{0.2-x}/GaP$ QW with pressure for different values of nitrogen mole fractions is presented in Figure 6.3. As can be seen from Figure 6.3, the strained band gap increases with pressure.

A reduction in the strained band gap appears with increasing N concentration. This reduction is related to the bowing in the band gap energy. It refers to the electronegativity and atomic radii between group V's anions. This behaviour is a result of the addition of N into III-V alloy semiconductor as an isoelectronic impurity [20].

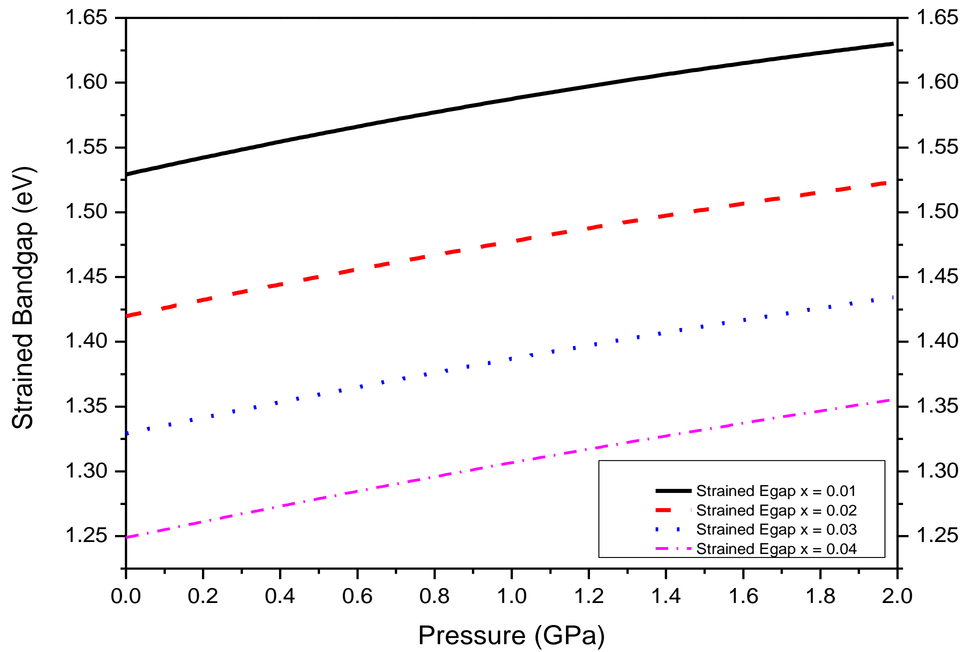

Figure 6.3: Strained band gap energy with pressure for different values of N concentration (x), $GaN_xAs_{0.8}P_{0.2-x}$/GaP QW.

6.3.3 Investigation of the pressure dependence of electron effective mass

The effective mass changes monotonically in conventional semiconductor with concentrations [54]. In novel alloy semiconductors, the incorporation of a small quantity of (~1%) of nitrogen into III-V alloys and compounds (e.g., GaP and GaAs, InGaAs) leads to drastically nonlinear adjustment in the band structure of the host lattice [55].

The band anti crossing model explains correctly the experimentally observed composition and pressure dependence of the III-N–V alloys band and expects several associated effects [56] such as the improvement of donor activation efficiency and the enhancement of the electron effective mass. The carriers effective masses with pressure provide valuable information on the basic nature of the band states in semiconductor [8] and are also critically significant for an investigation and optimization of III-N-V alloys in device application.

The lower subband E_- reduces the band gap energy. The flattening of the lower subband near its minimum leads to a large improvement of the electron effective mass [57].

Under hydrostatic pressure the energy gap increases with increasing pressure. The change in the band structure and changes in the ordering of the conduction band minima (CBM) results an increase in effective mass m*.

Figure 6.4 shows the increase in the electron effective mass with increasing pressure of $GaN_xAs_{0.8}P_{0.2-x}$/GaP QW. We calculate the electron effective mass using Eqn. (3.31) as a function of energy for different pressures. The pressure induced enhancement in the electron effective mass with different nitrogen concentrations in the alloy has been also calculated, and shown in Figure 6.4.

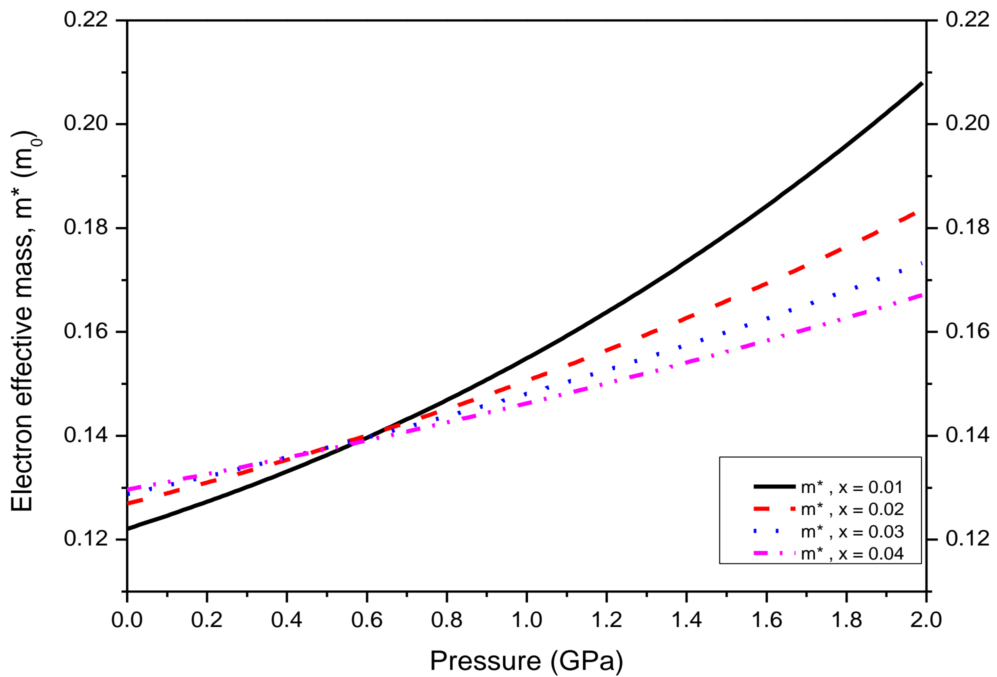

Figure 6.4: Electron effective mass as a function of pressure for various N concentrations.

The calculated effective mass increase with pressure is a result of the increase in the strained band gap with pressure. On the other hand the pressure dependence of the effective mass of $GaN_xAs_{0.8}P_{0.2-x}$ with different N concentrations is non-linear.

Effective mass increases with increasing N for small pressure values and vice versa for high pressure values.

Figure 6.6 shows both the nitrogen concentration and pressure dependence of the effective mass of electron in the same graph.

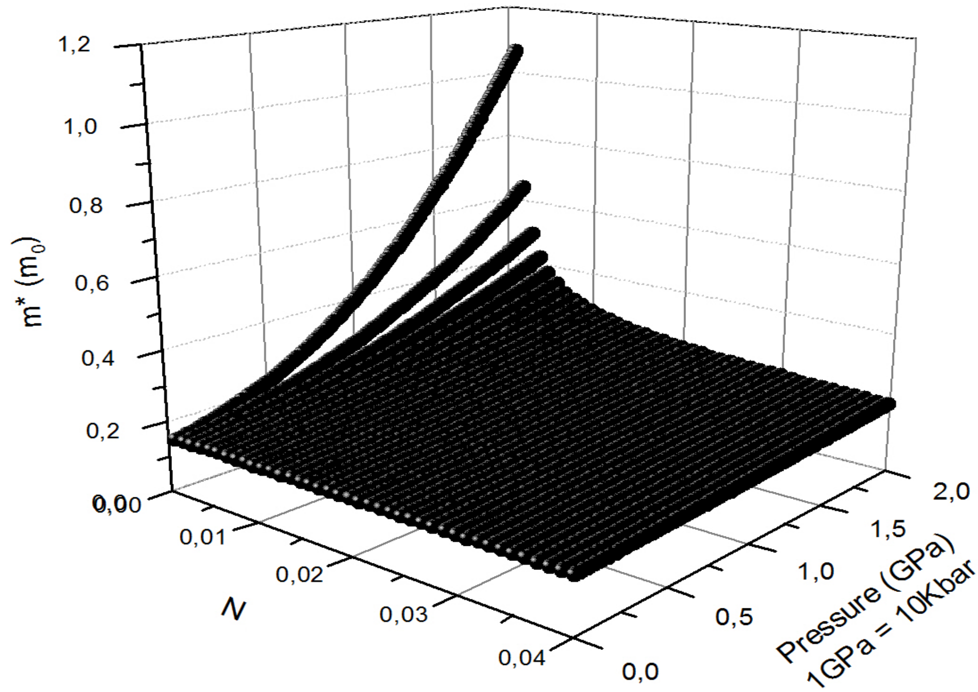

Figure 6.6: The calculated values of electron effective mass with increasing nitrogen and pressure for $GaN_xAs_{0.7}P_{0.3-x}$ QW on GaP substrate, according to BAC model

6.3.4 The analysis of the pressure dependence of non-radiative Auger recombination

The CHCC and CHSH Auger processes are the two dominant processes in the long wavelength devices. The expressions related to the pressure dependence of the non-radiative Auger recombination coefficient (C) are given in chapter 5. These equations based on parabolic bands and Boltzmann statistics. By means of using those expressions, we have calculated the pressure dependence of Auger losses in $GaN_xAs_{0.8}P_{0.2-x}$ on a GaP substrate for the first time. We have calculated that Auger losses decrease with increasing pressure.

6.3.4.1 Direct Auger processes (CHCC and CHSH)

Figure 6.7 shows the pressure dependence of direct Auger recombination (CHCC) for different N concentration (x). We have calculated that direct CHCC decreases sharply with pressure. This is due to the fact that strained band gap increases with pressure and Auger losses become insignificant since bands get further apart from each other. It is also seen from Figure 6.7 that that Auger losses become more important with increasing N concentration. This is again due to the fact that the bands get closer to each other with increasing N concentration. These results show that direct CHCC process depends strongly on the band parameters in $GaN_xAs_{0.8}P_{0.2-x}$ on GaP substrates.

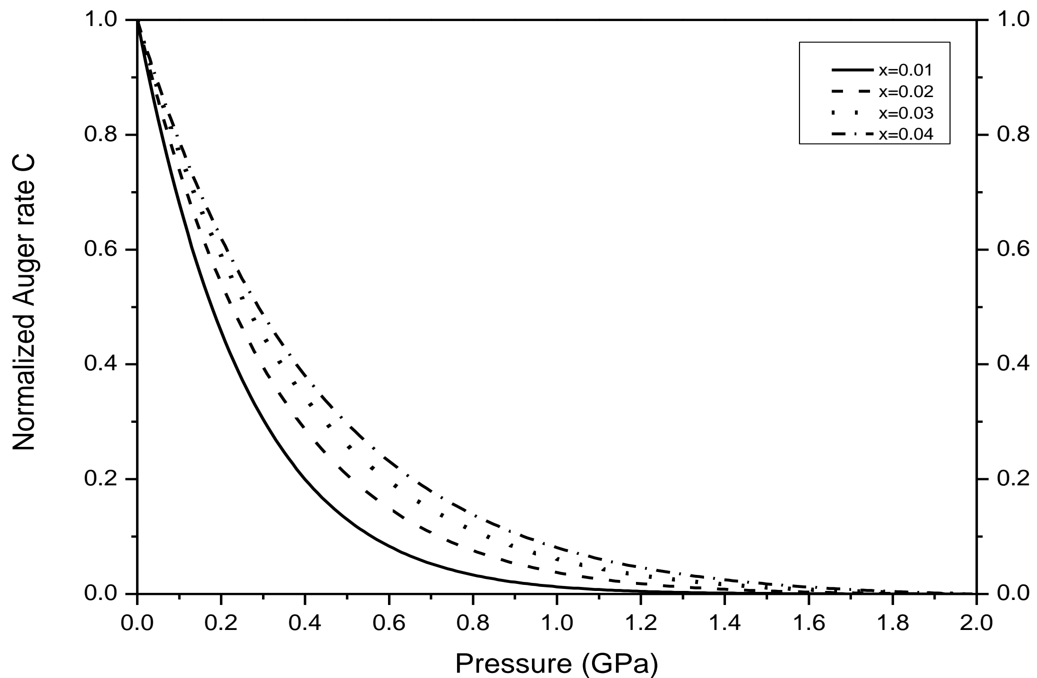

Figure 6.7: Direct Auger processes (CHCC) as a function of pressure for different values of N concentrations (x) in $GaN_xAs_{0.8}P_{0.2-x}$ on GaP substrate.

Figure 6.8 illustrates the calculated variation of the direct CHSH process with pressure in $GaN_xAs_{0.8}P_{0.2-x}$ on a GaP substrate. There is again a decrease in direct CHSH with pressure. However, the decrease is slower indicating that the direct CHSH process is less band structure dependent.

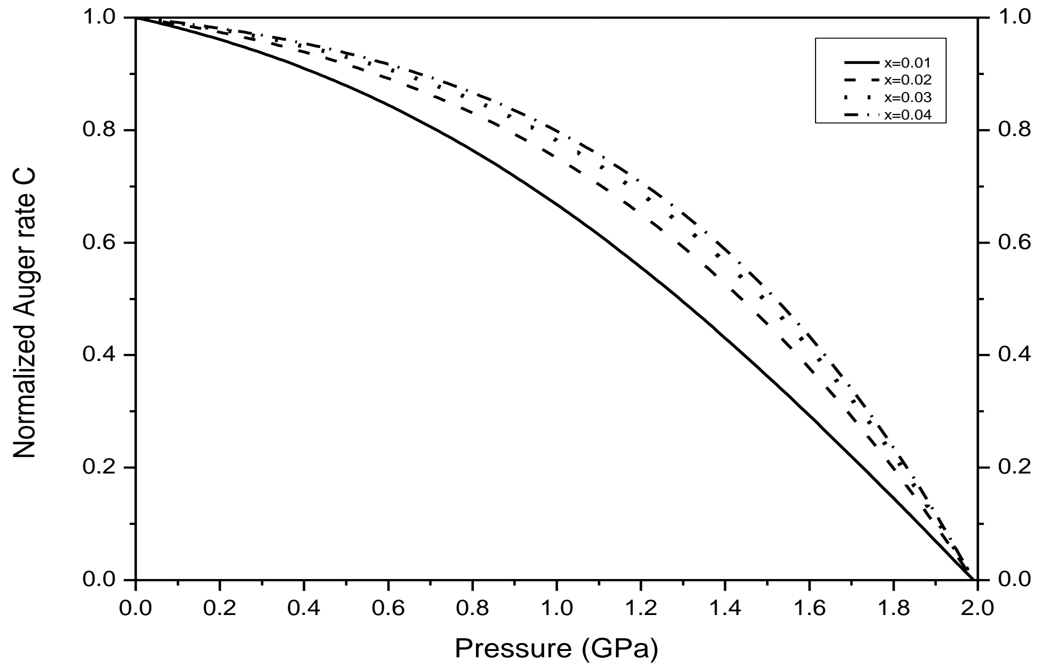

Figure 6.8: Direct Auger processes CHSH as a function of pressure with different N concentrations (x) $GaN_xAs_{0.8}P_{0.2-x}$ on a GaP substrate.

6.3.4.2 Phonon-assisted Auger processes (CHCC and CHSH)

We reveal the pressure dependence of phonon-assisted Auger processes in this section. Figures 6.9 and 6.10 show the calculated variation for phonon-assisted CHCC and CHSH processes, respectively. As it can be seen from both figures phonon-assisted CHCC and CHSH have a similar variation; both decreasing with increasing pressure. It is also seen from these figures that phonon-assisted processes are almost nitrogen independent.

Figure 6.11 summarizes the calculated variation of direct and phonon-assisted CHCC and CHSH processes for 1% nitrogen concentration. It is clear from Figure 6.11 that direct CHSH process is the dominant one and direct CHCC process is the less significant one in $GaN_xAs_{0.8}P_{0.2-x}$ on a GaP substrate.

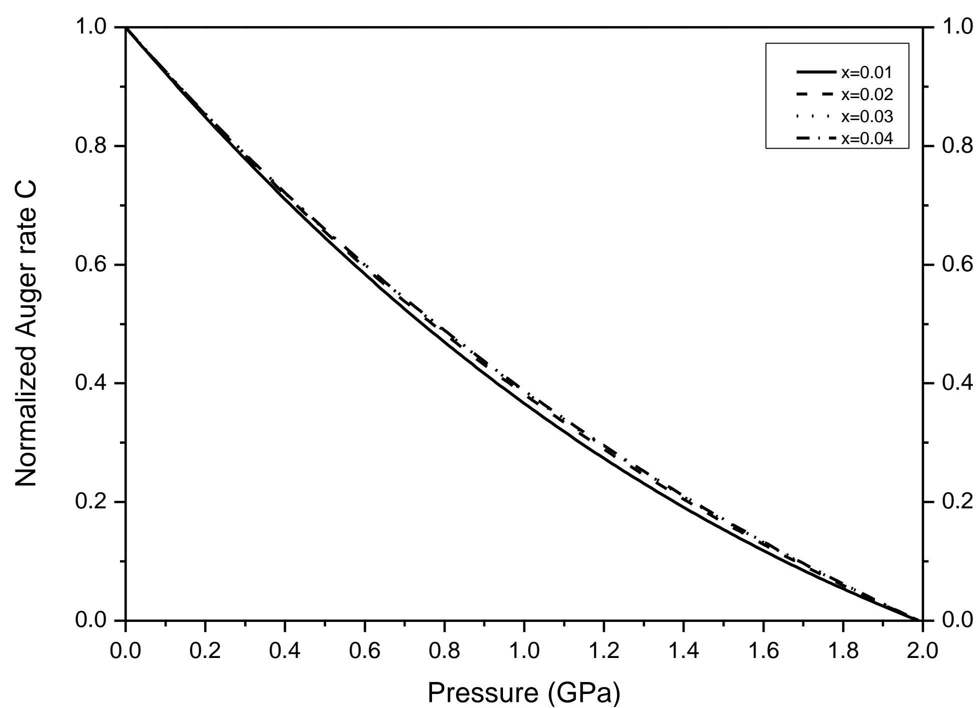

Figure 6.9: Phonon-assisted Auger processes CHCC as a function of pressure with different N concentrations (x).

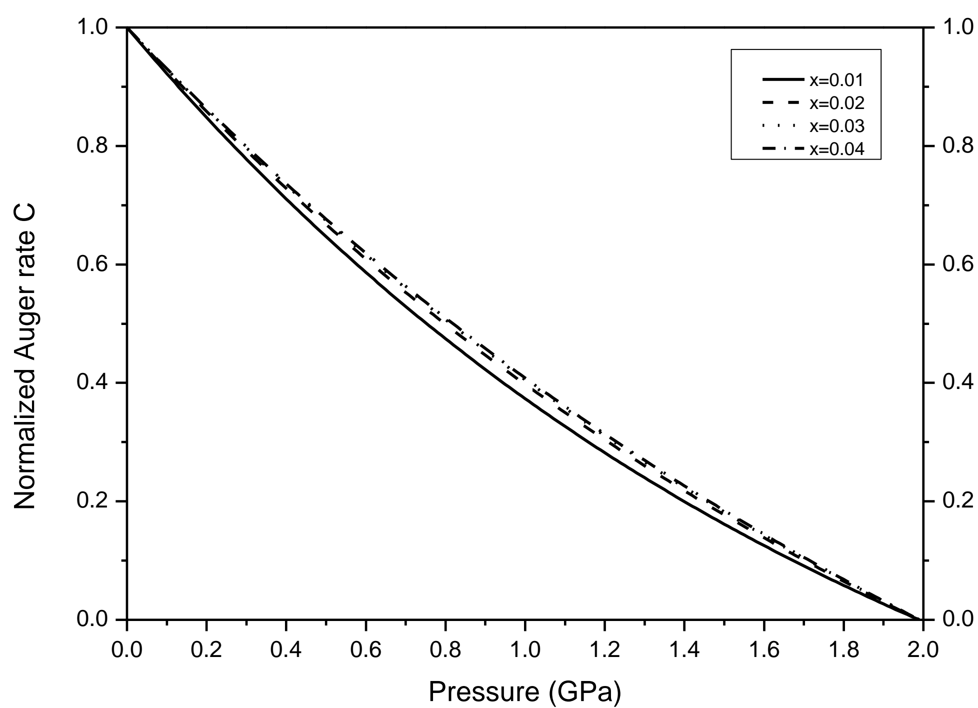

Figure 6.10: Phonon-assisted Auger processes CHSH as a function of pressure with different N concentrations (x).

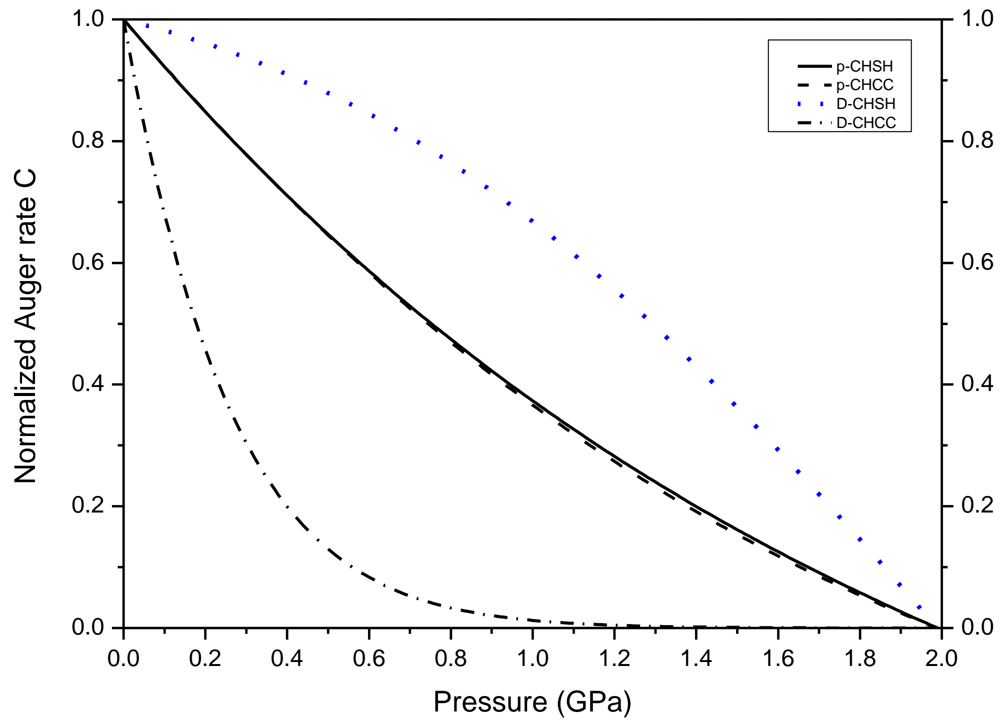

Figure 6.11: Auger processes (CHCC and CHSH) for both direct and phonon-assisted as a function of pressure with N concentrations (x=0.1).

CHAPTER 7

CONCLUSIONS

The III-N-V alloys are known as novel material system due to their unusual behaviour. These alloys are grown on GaAs and InP substrate conventionally. However these growths result strained materials and great attention must be paid while growing them. In recent years, people have considered GaP as a barrier material. The usage of GaP brings benefits since GaP is almost lattice-matched to silicon. Therefore, one can use the most available material, Si, as a substrate material in $GaN_xAs_{0.8}P_{0.2-x}$ / GaP QW laser systems.

It is known that hydrostatic pressure is one of the simplest techniques to vary continuously the band structure and determine the dominant loss mechanisms.

In this thesis study, we have revealed the pressure dependence of Auger losses in $GaN_xAs_{0.8}P_{0.2-x}$/GaP QW laser systems for the first time, up to our knowledge. To do that we first calculated the pressure dependences of band parameters. Then we have revealed the most important Auger recombination mechanisms. We have calculated that all Auger losses decrease with increasing pressure as expected. Our calculations indicate that phonon-assisted processes are almost nitrogen independent. These calculations reveal the fact that the direct CHSH mechanism is the most important loss mechanism in $GaN_xAs_{0.8}P_{0.2-x}$/GaP QW laser systems. On the other hand, direct CHCC mechanism is the less significant one in the same material system.

LIST OF REFRENCES

[1] Ruterana, P., Albrecht, M. and Neugebauer J. (2003). Nitride Semiconductors Handbook on Materials and Devices: 1st edition. Germany: WILEY-VCH Verlag GmbH and Co. KGaA,Weinheim.

[2] Buyanova, I.A., Chen, W.M. (2004). Physics and Applications of dilute nitrides New York London, Taylor & Francis.

[3] Erol, A. (2008). Dilute III-V Nitride Semiconductors and Material Systems. Vol.**105**.New York: Springer.

[4] Kunert, B., Reinhard, S., Koch, J., Lampalzer, M., Volz, K. and Stolz, W. (2006). *Physics Status Solidi.* C3, 614.

[5] Geisz, J.F. and Friedm, D.J. (2002). III–N–V semiconductors for solar photovoltaic applications. *Semiconductor Science Technology*. **17,** 769–777.

[6] Bakır, E. (2007). M.sc.thesis, Investigation of the Band Alignment of long-Wavelength InGa(N)As(Sb) Quantum wells on GaAs and InP Substrates. University of Gaziantep.

[7] Gönül, B. Ph.D Thesis, A Theoretical Study of the Threshold Current of Quantum Well Lasers. University of Surry (1995).

[8] Oduncuoğlu, M. (2004), Ph.D Thesis, A Theoretical Analysis of GaInNAs/GaAs Quantum Wells for Long Wavelength Emission. University of Gaziantep.

[9] Weyers, M., Sato, M., Ando, H. (1992), Red Shift of Photoluminescence and Absorption in Dilute GaAsN Alloy Layers, *Japanese Journal of Applied Physics*. 31, pp 853-855.

[10] Kondow M., Uomi K., Hosomi K. and Mozume T. (1994), Gas-Source Molecular Beam Epitaxy of GaNxAs1-x Using a N Radical as the N Source. *Japanese Journal of Applied Physics,* 33, pp.1056-1058.

[11] Walukiewicz, W., Shan, W., Ager, J.W., Chamberlin, D.R., Haller, E.E., Geisz, J.F, Friedman, D.J., Olson, J.M. and Kurtz, S.R. (1999), in

Photovoltaics for the 21 st Century, ed. by V.K. Kapur, R.D. McDonnell, D. Carlson, G.P. Ceasar, A. Rohatgi, (Electrochemical Society Press, Pennington, p. 190.

[12] Bi W.G. and Tu C. W. (1996), N incorporation in GaP and band gap bowing of GaN_xP_{1-x}. *Journal of Applied Physics*, **80**, 1934.

[13] Toivonen J., Hakkarainen, T., Sopanen M. and Lipsanen H. (2000), High nitrogen composition GaAsN by atmospheric pressure metalorganic vapor-phase epitaxy. *Journal of Crystal Growth*. **221**. pp 456 460.

[14] Perlin, P., Gorczyca, I. Porowski S. and Suski, T, (1993), III-V semiconducting Nitrides: Physical properties under pressure. *Japanese Journal of Applied Physics*. **32**, pp. 334-339.

[15] Shan, W., Walukiewicz, W.,Ager, J.W., Haller, E.E., Geisz, J.F., Friedman, D.J., Olson, J.M. and Kurtz, S.R. (1999), Band Anticrossing in GaInNAs Alloys. *Physical Review Letters*. **82,** pp. 1221-1224

[16] Christensen N.E., Gorczyca I., Svane1 A., Szwacki N.G., and Boguslawski P. (2003), Theoretical studies of semiconductors with and without defects under pressure. *Physica Status Solidi*, **2**, 374 – 383.

[17] Gorczyca, I., Christensen, N.E., Svane, A. (2005), Electronic structure of $GaAs_{1-x}N_x$ under pressure. *Solid State Community*, **136**, pp.439-449.

[18] Wu, J. , Shan, W. Walukiewicz, W. , Yu, K.M. , Ager, J. W., Haller, E.E. , Xin H.P. and Tu C. W. (2001), Effect of band anticrossing on the optical transitions in $GaAs_{1-x}N_x$/GaAs multiple quantum wells. *Physical Review B*, **64**.

[19] Gönül B. and Oduncuoğlu M. (2004), A theoretical comparison of the pressure dependence of the threshold current of phosphorus-, aluminium-andnitrogen-based 1.3 μm lasers. *Semiconductor Science Technology,* **19**, 23-32.

[20] Klar, P. J., Teubert, J., Güngerich, M., Niebling, T., Grüning, H., Heimbrodt, W., Volz, K., Stolz, W., Polimeni, A., Capizzi, M., O'Reilly, E.P., Lindsay, A., alluppi, M., Geelhaar, L., Riechert, H., and Tomić, S. (2007). Hydrostatic pressure experiments on dilute nitride alloys. *Physica Status Solidi*, **244**, 24-3.1.

[21] Chamings, J., Adams, A.R., Sweeney, S.J., Kunert, B., Volz, K., and Stolz W. (2008), Temperature dependence and physical properties of

Ga(NAsP)/GaP semiconductor lasers. *Applied Physics Letters*, **93**, pp.101-108.

[22] Skierbiszewski C., Perlin P., Wisniewski P., Suski T., Walukiewicz W., Shan W., Ager J.W., Haller E.E., Geisz J.F., Friedman D.J., Olson J.M., Kurtz S.R. (1999), Effect of Nitrogen-Induced Modification of the Conduction Band Structure on Electron Transport in GaAsN Alloys. *Physica Status Solidi B,* **216**, pp. 135–139.

[23] Hung, W.K., Cho, K.S., Chern, M.Y., and Chen, Y.F. (2001). Nitrogen-induced enhancement of the electron effective massin InN_xAs_{1-x}. *Applied Physics Letters*, **80**.

[24] Jin, S.R., Sweeney, S.J., Tomic, S., Adams, A.R., and Riechert H. (2003), High-Pressure Studies of Recombination Mechanisms in 1.3- m GaInNAs Quantum-Well Lasers. *Ieee Journal*, **9**.

[25] Massé, N.F., Adams, A.R., and Sweeney S.J. (2007), Experimental determination of the band gap dependence of Auger recombination in InGaAs/ InP multiple quantum well lasers at room temperature. *Applied Physics Letters*, **90**.

[26] Ellmers, C., Hofmann, M., W.Rühle, W., Girndt, A., Jahnke, F., Chow, W. W.Knorr, A., Koch, S.W., Hanke, C., Korte, L., and Hoyler, C. (1999), Gain Spectra of an (InGa)As Single Quantum Well Laser Diode. *Physica Status Solidi*, **206**, pp. 407–412.

[27] Vurgaftman, I., Meyer, J.R. and Ram, M.L.R, (2001), Band parameters for III–V compound semiconductors and their alloys. *Journal of Applied Physics*, **89**.

[28] Vurgaftman, I. and Meyer, J.R. (2003), Band parameters for nitrogen-containing semiconductors. *Japanese Journal of Applied Physics*, **94**.

[29] Jacob, K.T., Raj, S. and Rannesh, (2007), Vegard's law: a fundamental relation or an approximation. *International Journal of Materials Research*. pp. 776-779.

[30] Nishiyama, N., Lin, J., Okazaki, A., Iwasaka, M., Hirakawa, K. (1990), Vegard's Law in $KFe(S_{1-x}Se_x)_2$. *Japanese Journal of Applied Physics*, **29**, pp.369-371.

[31] Jin, Y. (2010), Influence Of N Incorporation On The Electronic Properties Of Dilute Nitride (IN)GaAsN ALLOYS, *Ph.D Thesis*, University of Michigan.

[32] URL http://environmentalchemistry.com/yogi/periodic/Ga.html.

[33] URL http://environmentalchemistry.com/yogi/periodic/In.html.

[34] Pauling L. (1932). The nature of the chemical bond. IV. the energy of single bonds and the relative electronegativity of atoms. *Journal of the American Chemical Society,* **54**, pp. 3570-3582.

[35] Palisaitis J., (2011), Electron Energy Loss Spectroscopy of III-Nitride Semiconductors, Linköping University., SE-58 183 Linköping: Sweden.

[36] Rockett A. (2008), The Materials Science of Semiconductors, *Springer.*

[37] de Walle C. G. (1989), Band lineups and deformation potentials in the model-solid theory. *Physical Review B,* **39**, pp.1871-1883.

[38] de Walle, C.G. and Martin, R.M.. (1987), Theoretical study of band offsets at semiconductor interfaces. *Physical Review,* **35**, pp.8154-8165.

[39] Baillargeon, J.N., Cheng, K.Y., Hofler, G.F., Pearah, P.J. and Hsieh, K.C., (1992), Luminescence quenching and the formation of the $GaP_{1-x}N_x$ alloy in GaP with increasing nitrogen content. *Applied Physics Letters*, 60, pp.2540-2542.

[40] Ager, J., Walukiewicz, W. and Yu, W.K.M. (2006), Ultrahigh efficiency multiband solar cell. *Lawrence Berkeley National Laboratory*, LBNL Report 59768, LBNL Report 59768.

[41] Adachi S., (1994), GaAs and Related Materials: Bulk Semiconducting and Su-perlattice Properties World Scientific, Singapore.

[42] Jappor, H.R. (2011). Band-Structure Calculations of GaAs within Semiempirical Large Unit Cell Method. *European Journal of Scientific Research,* **59**.

[43] URL http://en.wikipedia.org/wiki/File:Gallium-arsenide-unit-cell-3D-lls.png

[44] URL http://en.wikipedia.org/wiki/Gallium_phosphide

[45] URL http://en.wikipedia.org/wiki/File:Sphalerite-unit-cell-3D-balls.png

[46] Narayanamurti, V. (2003), Growth and Characterization of GaN As(P) for High Efficiency Solar Cells, Harford University. National Renewabl e Energy La boratory.

[47] Schubert, E.F. (2006). Light-Emitting Diodes, 2nd Edition, United States of America, Cambridge University Press.

[48] Yonezu H. (2002). Control of structural defects in group III–V–N alloys grown on Si. *Semiconductor Science Technology,* **17**, 762.

[49] Christina, B., Kuhn, E., Schlichenmaier, C., Imhof, S., Thra¨ nhardt, A., Hader, Jorg, Jerome, V.M., Rubel O., Zhang W., Ackemann T., and Koch S. W.. (2010). Quantum modeling of semiconductor gain materials and vertical-external-cavity surface-emitting laser systems. *Physica Status Solidi*, **247**, 789–808.

[50] Henini, M. (2005). Dilute Nitride Semiconductors, 1st Edition, *Elsevier,* UK.

[51] URL http://www.ioffe.ru/SVA/NSM/Auger/model.html

[52] Haug, A. (1992). Auger recombination in quantum well semiconductors: calculation with realistic energy bands. *Semiconductor Science Technology*, **7**, 1337.

[53] Adachi, S. (1992). Physical Properties of Ш-V Semiconductor Compounds InP, InAs, GaAs, GaP, InGaAs, and InGaAsP , JOHN WILEY & SONS.

[54] Börnstein L. and Madelung O., Ed. (1987). Numerical Data and Functional Relationships in Science and Technology. *Berlin Springer Verlag*, **22**.

[55] Masia, F., Pettinari, G., Polimeni, A., Felici, M., Miriametro, A. and Capizzi, M. (2006). Interaction between conduction band edge and nitrogen states probed by carrier effective-mass measurements in $GaAs_{1-x}N_x$. *Physical Review B,* **73**, 073201.

[56] Cánovas, E., Martí, A., Luque, A. and Walukiewicz, W. (2008). Optimum nitride concentration in multiband III-N–V alloys for high efficiency ideal solar cells, *Applied Physics Letters*, **93**.

[57] Hader J., Koch S.W., Moleney J.V., Reilly E.P. (2000). Gain in 1.3 μm materials: InGaNAs and InGaPAs semiconductor quantum-well lasers. *Applied Physics Letters,* **77**, 630.